Mon. Not. R. Astron. Soc. **260,** 221–240 (1993)

Modelling of X-ray emission from WR + O binary systems

A. V. Myasnikov[1] and S. A. Zhekov[2]★

[1] *Institute for Problems in Mechanics, Russian Academy of Sciences, Prospekt Vernadskogo 101, Moscow 117526, Russia*
[2] *Space Research Institute, Division of High Energy Astrophysics, Moskovska str. 6, Sofia 1000, Bulgaria*

Accepted 1992 June 26. Received 1992 May 15; in original form 1992 January 13

ABSTRACT

Two-dimensional calculations of colliding stellar winds are performed for the case of a WR + O binary system. The effects of energy losses by free–free emission and Comptonization as well as those of stellar wind acceleration are considered. The results show that the interaction region must be a powerful X-ray source. The main dimensional parameters determining the X-ray spectrum and the luminosity of a WR + O binary system are the stellar mass losses, the wind velocities, the separation between the stars and their chemical composition (the X-ray emission characteristics of WN + O and WC + O systems are very different). An investigation of energy losses due to free–free emission shows that radiative losses may play an important role in the physics of the interaction region if all the thermal processes are included (free–free, two-photon and recombination continua, and emission lines). In this case, the thermal conductivity must be taken into account in the modelling of colliding stellar winds. The closer the binary system, the more important is the role of energy losses by thermal emission and Comptonization. The effects of stellar wind acceleration are also important for close WR + O binary systems in which the contribution of the shocked O-star wind gas to the total X-ray emission may be dominant.

Key words: MHD – binaries: close – stars: mass-loss – stars: Wolf–Rayet – X-rays: stars.

1 INTRODUCTION

Studies of Wolf–Rayet (WR) stars show that about 40 per cent of them are binary systems (Conti 1988). On the basis of the similarity of the optical spectra of WR and novae stars, Beals proposed a model of an outflowing atmosphere and stellar wind (Beals 1929). Moreover, it was noted by Cherepashchuk (1967) that, in a binary system containing a WR star plus another star, X-ray emission from hot gas (10^7–10^8 K) can originate in a shock layer when the WR stellar wind interacts with the surface of its companion. The interaction of the WR wind with the magnetosphere (or the stellar wind) of the companion star was investigated by Prilutskii & Usov (1976), who proposed an approximate formula for the X-ray luminosity in these cases. Using their result, Cherepashchuk (1976) calculated the X-ray luminosities of some WR + O binary systems and estimated the role of energy losses by Comptonization. His estimates showed that the expected X-ray luminosities are in the range $L_x \approx 10^{32}$–10^{34} erg s^{-1} for a mass-loss rate from the WR star of $\dot{M}_{WR} \approx 10^{-6}$–$10^{-5}$ $M_\odot$ yr^{-1}. In addition, the X-ray fluxes from these systems should vary in time due to the eclipse of the interaction region by the WR and O stars or their atmospheres (winds). Bajramov, Pilyugin & Usov (1988, 1990) made more accurate estimates of the X-ray luminosity by considering energy losses by free–free emission with the help of the thin-slab approximation (Chernij 1959).

The interaction of two radial stellar winds was examined qualitatively for the first time by Siscoe & Heinemann (1974). They considered the effects of the relative stellar separation on the initial geometrical picture, and tried to take into account the roles of the magnetic fields and the stellar rotation and the effects of the orbital motion. Girard & Wilson (1987) used the model of colliding radial flows for the case of erupting symbiotic stars. Shore & Brown (1988) applied it to the interpretation of ultraviolet (UV) observations of the WR + O binary system V444 Cygni. In both papers, the approximate form of the shock region was determined by using the momentum balance in a thin slab of the interacting gas. Kallrath (1991) investigated the dynamical and geometrical aspects of two quasi-radial colliding gas flows in the framework of pressure equilibrium models.

★ Present address: Arcetri Astrophysical Observatory, Largo Enrico Fermi 5, 50125 Florence, Italy.

The exact structure of the interaction region of two colliding radial winds (without energy losses due to radiative processes) was determined by Lebedev & Myasnikov (1988, 1990), using a numerical solution of the two-dimensional Euler equations solved with the help of the finite-difference method of Babenko & Rusanov (1965). Lebedev & Myasnikov made a parametric investigation of their results and formulated transition conditions for some asymptotic flows, particularly for the case of an interaction between a radial and a uniform (linear) gas flow. On the basis of these results, the X-ray luminosity of V444 Cyg was estimated taking into account only free–free emission of the shocked gas. These numerical simulations were used by Zhekov & Myasnikov (1989) to calculate the detailed X-ray spectrum and the luminosity of V444 Cyg in the framework of the Raymond & Smith (1977) model of radiation emitted by a hot optically thin plasma. A preliminary attempt to take into account the effect of radiation and Comptonization energy losses on the structure of the stellar wind interaction region is given in Myasnikov & Zhekov (1990, 1991). In addition, numerical simulations of the interaction of two stellar winds have been made by Luo, McCray & MacLow (1990) for the cases of HD 165052 (two identical winds in an O+O binary system) and V444 Cyg (one dominant wind).

All of the exact and approximate estimates of the X-ray luminosities of WR+O binary systems are 10–100 times greater than the observed values (e.g. Moffat et al. 1982; Pollock 1987) (except for the results of Luo et al. (1990), which are consistent with the observations). In order to remove this significant discrepancy, Pollock (1987) suggested that much of the X-ray emission from the shocked gas is probably absorbed by the overabundant elements C, N and O in the WR wind. Furthermore, Cherepashchuk (1990) developed the idea of a cloudy structure for the stellar wind and proposed that about 80 per cent of the wind mass is held in dense collisionless cloudlets, which make an insignificant contribution to the X-ray emission, so the X-ray emission originates in the interaction of the continuous components of both gas flows.

The purpose of our paper is to determine the structure and X-ray characteristics of the interaction region of colliding stellar winds, taking into account the influence of stellar wind acceleration and energy losses by radiation and Comptonization, as well as the different chemical compositions of stars.

We describe the gas dynamical problem in Section 2. Numerical results for the structure of the stellar wind interaction region are given in Section 3. In Section 4 we calculate characteristics of the X-ray emission (spectrum, luminosity, etc.) of a 'standard' WR+O binary system, taking into account different chemical compositions (WN or WC), energy losses by free–free emission and by Comptonization, effects of stellar wind acceleration, and X-ray absorption in O and WR stellar atmospheres (winds). The astrophysical results are discussed in Section 5. The main conclusions are presented in Section 6.

2 GAS DYNAMICAL PROBLEM

The gas flows (winds) from both stars in a WR+O binary system have spherical symmetry, so the dynamical problem of colliding stellar winds will have axial symmetry if the effects of orbital motion are neglected. This criterion is fulfilled when stellar magnetic fields and stellar rotation do not influence the gas dynamics, and typical orbital velocities ($V_{\rm orb} \approx 100$–300 km s^{-1}) are much less than the characteristic velocity for the problem under consideration (this characteristic velocity is the typical stellar wind velocity in WR+O binary systems, $V_{\rm w} \approx 2000$–3000 km s^{-1}). This assumption is valid for almost all the WR+O binary systems except the closest ones, in which the WR wind may suppress the O-star wind in front of the interaction region. The effects of Coriolis forces must be included in the solution for these systems. In this paper we shall study the effects of stellar wind acceleration only in the case for which the orbital motion can be neglected (i.e. excluding very close binary systems such as V444 Cyg, CQ Cep, CX Cep, etc.).

The interaction of two spherical radial gas flows is characterized by the relative stellar separation of the binary system $(R_{*1}+R_{*2})/2D$ (Siscoe & Heinemann 1974), where R_{*1} and R_{*2} are the critical radii of the stars (i.e. the radii at which the gas velocity equals the sound velocity) and $2D$ is the separation between them. The values of R_{*1} and R_{*2} and, consequently, the relative stellar separation depend on many physical characteristics of both stars (particularly on their masses, luminosities, etc.) – this is why we choose R_{*1} and R_{*2} to be parameters for the problem under consideration.

In the model of an inviscid gas having no thermal conductivity (which is appropriate for large Reynolds numbers), the stellar flow region consists of the following parts (illustrated in Fig. 1): an interaction region delimited by the shocks F and G, and divided into two parts (I and II) by the contact discontinuity S; and regions III and IV of the free-flowing stellar winds. In regions I and II the gas flow is described by the

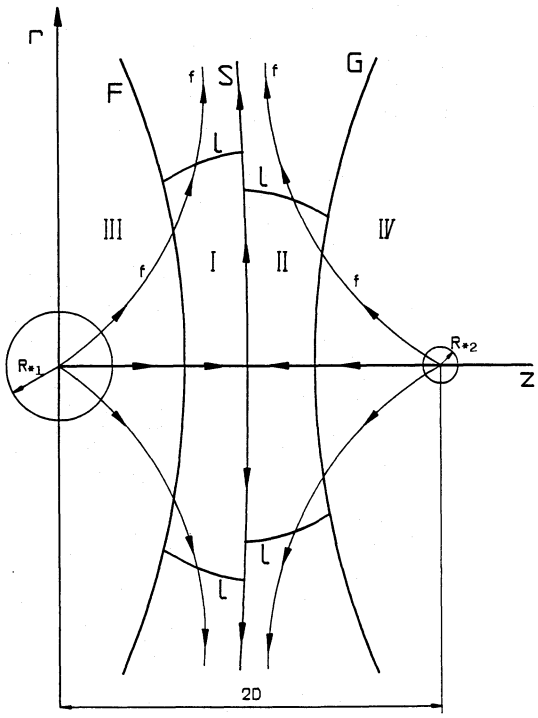

Figure 1. A schematic diagram of the interaction between two supersonic radial flows. *F*, *G* – shock waves: *S* – contact discontinuity; *l* – sonic lines; *f* – stream-lines; R_{*1}, R_{*2} – radii of stars; $2D$ – separation between the two stars.

Euler equations:

$$\nabla\cdot\rho\boldsymbol{v}=0,$$
$$\rho(\boldsymbol{v}\cdot\nabla)\boldsymbol{v}+\nabla p=0, \qquad (1)$$
$$\boldsymbol{v}\cdot\nabla p+\gamma p\nabla\cdot\boldsymbol{v}=-(\gamma-1)(Q_{\rm ff}+Q_{\rm c}),$$

where ρ, p and $\boldsymbol{v}$ are the gas density, pressure and velocity in the interaction region, and γ is the adiabatic index in regions I and II.

The terms on the right-hand side of the energy equation characterize energy losses by free–free emission (Allen 1973) and Comptonization (Levich & Sunyaev 1971):

$$Q_{\rm ff}=1.44\times10^{-27}T_{\rm e}^{1/2}n_{\rm e}g\sum_Z n_Z Z^2\ {\rm erg\ cm^{-3}\ s^{-1}}, \qquad (2)$$

$$Q_{\rm c}=\frac{4\sigma_T kT_{\rm e}n_{\rm e}}{m_{\rm e}c}(\varepsilon_1+\varepsilon_2)\ {\rm erg\ cm^{-3}\ s^{-1}},$$

where g is the Gaunt factor, $\sigma_{\rm T}$ is the Thomson scattering coefficient, k is Boltzmann's constant, $m_{\rm e}$ is the electron mass, c is the speed of light, and ε_1 and ε_2 are the radiation densities of the two stars: $\varepsilon_i=L_i/4\pi cR_i^2$, $i=1,2$, where L_i is the luminosity and R_i is the distance to the ith star.

The number densities of electrons and ions and the electron temperature are connected to the density ρ and the pressure p by the following relations:

$$n_{\rm e}=n_{\rm tot}\sum_Z X_Z Z=\frac{\rho}{\bar{\mu}m_{\rm p}}\sum_Z X_Z Z,$$
$$n_Z=X_Z n_{\rm tot}=\rho\frac{X_Z}{\bar{\mu}m_{\rm p}}, \qquad (3)$$
$$T_{\rm e}=T=\frac{\mu}{R}\frac{p}{\rho},$$

where $m_{\rm p}$ is the proton mass, X_Z is the relative number density of an ion having a charge Z, $\bar{\mu}$ is the mean atomic weight of the nucleon, $\mu=\bar{\mu}/(1+\sum X_Z Z)$ is the mean atomic weight of the electron + nucleon mixture, and R is the gas constant.

Free–free emission and Comptonization influence the structure of the interaction region if the characteristic time-scales for these processes,

$$\tau_{\rm ff}=2.1\times10^{27}\,kT^{1/2}n^{-1}\ {\rm s}$$

and

$$\tau_{\rm c}=\frac{3}{4}\frac{mc}{\sigma_{\rm T}(\varepsilon_1+\varepsilon_2)}\ {\rm s}$$

are comparable to the characteristic time-scale of the gas dynamics, $\tau=D/V_\infty$ (V_∞ is the wind velocity). When $\tau_{\rm ff}$ and $\tau_{\rm c}$ exceed the time-scale for equalization of the electron and ion temperatures, $\tau_{\rm ei}=6T^{3/2}n^{-1}$(s) (Spitzer 1962), we can neglect the energy losses in relaxation zones (slabs) modelled by the shock discontinuities F and G, and instead use the standard Rankine–Hugoniot equations relating the solutions of (1) in regions I and II, on the one hand, and the parameters of the free-blown winds in regions III and IV, on the other hand:

$$\rho_+ v_+^{(\rm n)}=\rho_- v_-^{(\rm n)}, \qquad v_+^{(\rm t)}=v_-^{(\rm t)},$$
$$\rho_+[v_+^{(\rm n)}]^2+p_+=\rho_-[v_-^{(\rm n)}]^2+p_-,$$
$$\frac{\gamma}{\gamma-1}\frac{p_+}{\rho_+}+\frac{1}{2}v_+^2=\frac{\gamma}{\gamma-1}\frac{p_-}{\rho_-}+\frac{1}{2}v_-^2, \qquad (4)$$

where the subscript '−' denotes the values in front of the shocks, '+' denotes those behind it, and $v^{(\rm n)}$ and $v^{(\rm t)}$ are the normal and the tangential components of flow velocity $\boldsymbol{v}$, respectively. On the contact discontinuity the following relations are valid for the solutions of (1) in regions I and II:

$$v_{\rm I}^{(\rm n)}=v_{\rm II}^{(\rm n)}, \qquad p_{\rm I}=p_{\rm II}, \qquad (5)$$

the gas is non-flowing, and the gas pressures are equal. In fact, the parameters of free-flowing winds have to be determined by the solutions of the gas dynamical problem, which give the structure of an outflowing stellar atmosphere, taking into account radiative transfer in a moving medium. To determine the structure of the interaction region, which interests us, it is only necessary to know the wind parameters in front of the shocks F and G. This is why, in previous studies of the interaction region and its X-ray emission, it was assumed that the wind velocities are equal to their terminal values v_∞ (Lebedev & Myasnikov 1988, 1990; Zhekov & Myasnikov 1989; Myasnikov & Zhekov 1990) or differ slightly from them (Myasnikov & Zhekov 1991). This approximation is valid for wide binary systems where the wind dynamic pressures are not too different. In contrast, in a WR + O system the more powerful WR wind will suppress the O-star wind, which will not be able to reach its terminal velocity. In order to take this effect into account we use a wind velocity which obeys the following law:

$$v=v_0+(v_\infty-v_0)\left(1-\frac{R_*}{R}\right)^\beta, \qquad (6)$$

where β is a parameter, R is the distance from the star, v_0 is the velocity at the transonic (critical) point [$v_0=v(R_*)=a_{\rm s}$, $a_{\rm s}$ is the sound speed] and v_∞ is the terminal wind velocity.

If we normalize all the linear sizes to D (where $2D$ is the distance between the stars), all the velocities to the terminal wind velocity $v_{1\infty}$ of the first star, and the densities and pressures to $\dot{M}_1/4\pi v_{1\infty}D^2$ and $\dot{M}_1 v_{1\infty}/4\pi D^2$, respectively, the dimensionless hydrodynamical equations for the free-flowing gas in region III are

$$\rho UR_1^2=1,$$
$$U=W+(1-W)\left(1-\frac{K_1}{R}\right)^\beta, \qquad (7)$$
$$p=\frac{1}{\alpha_1}\rho^{\alpha_1}W^{1+\alpha_1}K_1^{2(\alpha_1-1)}.$$

For the same normalizations, the dimensionless hydrodynamical equations in region IV are

$$\rho UR_2^2=\dot{M},$$

$$U = W\chi + \chi\left(\frac{X}{\chi} - W\right)\left(1 - \frac{K_2}{R}\right)^{\beta}, \tag{8}$$

$$p = \frac{1}{\alpha_2}\rho^{\alpha_2} W^{1+\alpha_2} K_2^{2(\alpha_2-1)} \dot{M}^{1-\alpha_2} \chi^{1+\alpha_2}.$$

In equations (7) and (8), $K_1 = R_{*1}/D$, $K_2 = R_{*2}/D$, $\dot{M} = \dot{M}_2/\dot{M}_1$, $X = v_{2\infty}/v_{1\infty}$, $\chi = a_2/a_1$ and $W = a_1/v_{1\infty}$. $v_{1\infty}$ and $v_{2\infty}$ are the terminal velocities of both winds, a_1 and a_2 are their critical velocities, and α_1 and α_2 are the polytropic indices for both winds, which are usually different. We assume in our calculations that $X = \chi$ and $\alpha_1 = \alpha_2 = 1.1$. The values of α_1 and α_2 correspond to the modelling of the gas flow as quasi-isothermal.

Applying the same procedure as above, the first two equations in (1) and the boundary conditions (4), (5) keep their form, and the third equation in (1) is rewritten as

$$\boldsymbol{v}\cdot\nabla p + \gamma p \nabla\cdot\boldsymbol{v} = -(\gamma-1)\left[\Gamma_{\rm ff} p^{1/2}\rho^{3/2} + \Gamma_{\rm c} p\left(\frac{1}{R_1^2} + \frac{L}{R_2^2}\right)\right], \tag{9}$$

where

$$\Gamma_{\rm ff} = 0.31\,\omega\,\frac{\dot{M}_{1(6)}}{D_{(12)} v_{1(8)}^3}, \qquad \Gamma_{\rm c} = 0.26\,\delta\,\frac{L_{1(38)}}{D_{(12)} v_{1(8)}},$$

$$\omega = \frac{\mu^{1/2}(2-\chi_{\rm H})Z^2}{\bar{\mu}^2}, \qquad \delta = \frac{\mu}{\bar{\mu}}(2-\chi_{\rm H}),$$

are dimensionless parameters related to the characteristic times $\tau_{\rm ff}$, $\tau_{\rm c}$ and τ as follows:

$$\Gamma_{\rm ff} \approx \frac{\tau}{\tau_{\rm ff}}, \qquad \Gamma_{\rm c} \approx \frac{\tau}{\tau_{\rm c}}.$$

Here, $\dot{M}_{1(16)} = \dot{M}_1/10^{-6}\,{\rm M}_\odot\ {\rm yr}^{-1}$, $v_{1(8)} = v_{1\infty}/10^8$ cm s^{-1}, $D_{(12)} = D/10^{12}$ cm, $L_{(38)} = L_1/10^{38}$ erg s^{-1}, $L = L_2/L_1$ and $\chi_{\rm H}$ is the relative number density of hydrogen.

The gas dynamical simulations assume that the wind of star 1 consists of fully ionized hydrogen, and that of star 2 of fully ionized helium. So $\omega_{\rm I} = 0.50$, $\omega_{\rm II} = 0.58$, $\delta_{\rm I} = 0.5$, $\delta_{\rm II} = 0.67$ and the coefficients $\Gamma_{\rm ff}$ and $\Gamma_{\rm c}$ have different values in regions I and II.

Each of the regions I and II consists of a subsonic part (around the axis of symmetry) and a supersonic one (downstream), bounded by the sonic line l (Fig. 1), and the corresponding solutions can be obtained sequentially.

First, for the subsonic part of the interaction region ($r \le r_0$), the dynamical problem can be solved numerically with the help of the finite-difference relaxation method of Babenko & Rusanov (1965), which is widely used in calculations of streamlined blunt bodies, and which was modified by Lebedev & Sandomirskaya (1981) for the case of gas flows having three discontinuity surfaces. In this case r_0 is chosen such that the sonic line is entirely situated in the region having r-dimension smaller than r_0, so the boundary conditions are not necessary at $r = r_0$. Secondly, when the solution of the gas dynamical problem in the subsonic region allows the existence of r_1 such that $r_1 \le r_0$, and a system of equations (1) of r-hyperbolic type at $r \ge r_1$, then the solution can be continued into the supersonic region with the help of the steady-state modification of the Babenko–Rusanov method (the 'marching' method: see Dyakonov & Uskov 1970). Results derived by the relaxation method and those derived by the 'marching' method in the region defined by $r_1 \le r \le r_0$ usually differ from each other by less than 3 per cent, and this gives an estimate of the accuracy of the solutions. In order to estimate the accuracy of our results, we compared the inflowing and the outflowing masses of the gas in the interaction region, and we also verified some relations following from the equations solved (although not from the finite-difference method). The estimated accuracy was satisfactory.

3 STRUCTURE OF THE INTERACTION REGION

The interaction of supersonic stellar winds is entirely determined by the following parameters: $\dot{M}$, χ, γ, $\Gamma_{\rm ff}$ and $\Gamma_{\rm c}$. It was demonstrated by Lebedev & Myasnikov (1988, 1990) that when $\Gamma_{\rm ff}$, $\Gamma_{\rm c} = 0$ the geometric structure of the interaction region depends on the parameters $\Lambda = \dot{M}\chi$ and γ. The parameter χ exerts an influence only on the dimensionless velocity and density in region II, and their new values can be derived and simply scaled on the basis of an existing solution. Lebedev & Myasnikov (1990) showed that, when the gas dynamical pressures are almost equal ($\Lambda \ge 1$), all the discontinuity surfaces F, S and G become linear at distances far from the axis of symmetry. The opposite case ($\Lambda \gg 1$) is shown in Fig. 2 and demonstrates that with the increment of Λ the inner shock F is forced closer to the axis of centres, forming a flat shock–Mach disc behind which the gas flow is subsonic again. The outer shock G and the contact discontinuity S keep their asymptotic linear form. Similar structures were considered by Shima, Matsuda & Inaguchi (1986) in their numerical simulations of the interaction of radial and uniform (linear) gas flows. They considered an asymptotic

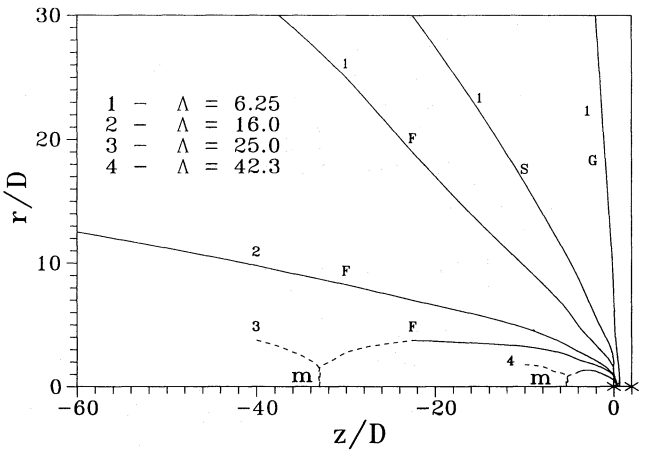

Figure 2. The geometrical structure of the supersonic part of the interaction region. The dashed line shows the theoretical behaviour (not calculated by us) of the inner shock. *m* – Mach disc; *F* and *G* – inner and outer shocks, respectively; *S* – contact discontinuity.

case of our gas dynamical problem, with $D \gg R$ and $\Lambda \gg 1$ (Lebedev & Myasnikov 1990).

3.1 Energy losses by free–free emission and Comptonization

As noted above, the energy losses in radiative processes can substantially influence the interaction region of colliding stellar winds in a close binary system. An approximation of volume emissivity is often used in calculations of similar effects in models of blunt bodies stream-lined by a radiating supersonic gas flow. To take into account radiative heat-exchange losses in this approximation, an appropriate term in the energy equation for inviscid non-heat-conducting gas is added. Its value depends on the gas thermodynamic parameters. In the case of a simple one-dimensional model of the gas flow, the behaviour of this term has been investigated at the stagnation point with the help of an integro–differential equation derived after some simplifications (Coulard 1964; Thomas 1965; Vertushkin & Zhigulev 1967). The solution of this equation shows that the temperature is zero at the stagnation point in the cases of optically thin and optically thick gas. This singularity is the result of the fact that the gas particle moving along the critical stream-line to the body has been decelerated for an infinitely long time, and for this reason the gas has emitted all of its internal energy. Taking into account higher order terms in the cases of optically thick (Thomas 1965) and optically thin (Vertushkin & Zhigulev 1967) gas, this singularity can be eliminated by using the concept of the viscid heat-conducting shock layer (Bogopelov & Neiland 1966). In addition, the energy-balance behaviour of an emitting and absorbing gas particle which moves along the zero stream-line has been determined (Vertushkin & Zhigulev 1967; Stulov & Shapiro 1969): this particle emits an amount of energy equal to that derived from the total gas volume. Using this condition, it becomes possible to carry out two-dimensional calculations in the frame of the Euler equations, by applying the volume emissivity approximation (Stulov & Shapiro 1970).

As our previous calculations showed (Myasnikov & Zhekov 1991), the singularity might also be eliminated at the expense of numerical viscosity, equivalent to some fictitious dissipating process. In accordance with these calculations, cooling due to radiation does not influence the pressure distribution and the normal velocity component at the contact discontinuity. However, the density distribution (Fig. 3) and the tangential velocity component at the contact discontinuity depend strongly on the coefficients Γ_{ff} and Γ_c. This influence of radiation on a shocked gas flow is typical of the volume emissivity approximation, and does not depend on the exact form of the term added into the energy equation (Stulov & Shapiro 1970). However, the particular form of Q_{ff}

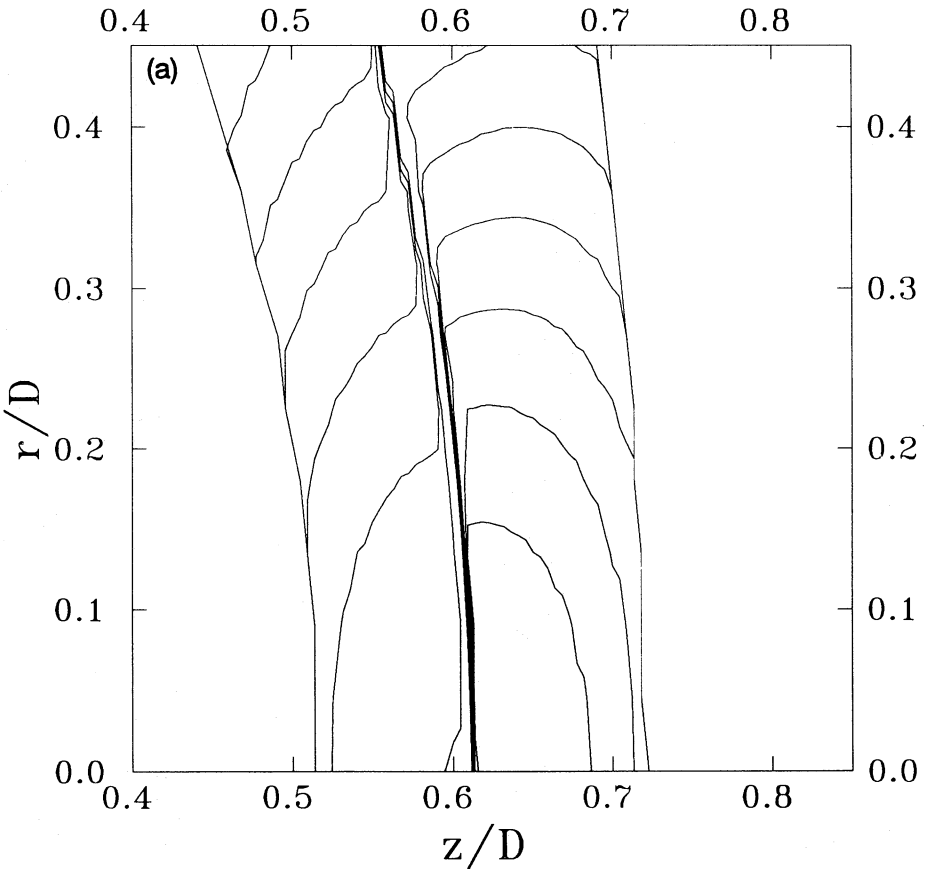

Figure 3. Isochores in the interaction region in the case with $\Lambda = 6.25$, $\chi = 0.78$, $K_1 = K_2 = 0$. (a) $\Gamma_{ff} = \Gamma_c = 0$; (b) $\Gamma_{ff} = 0$, $\Gamma_c = 0.125$; (c) $\Gamma_{ff} = 0.125$, $\Gamma_c = 0$. The maximum values are found near the axis of symmetry, z. The unresolved zone close to the contact discontinuity (b and c) is due to the large gradients.

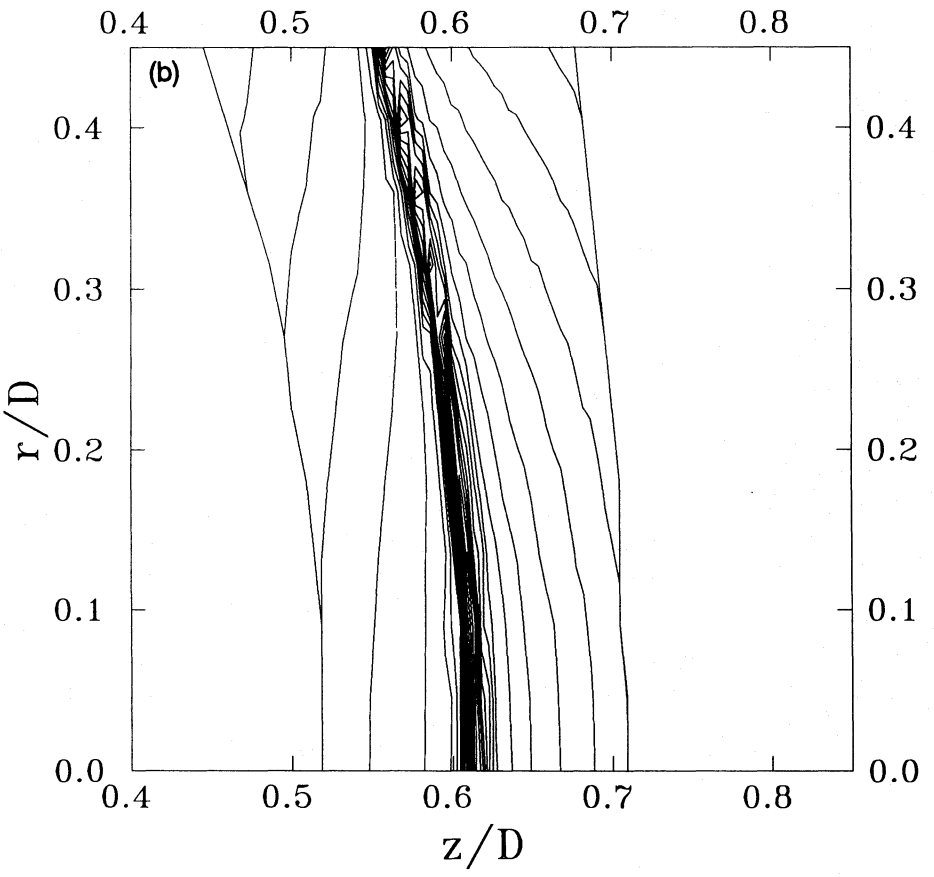

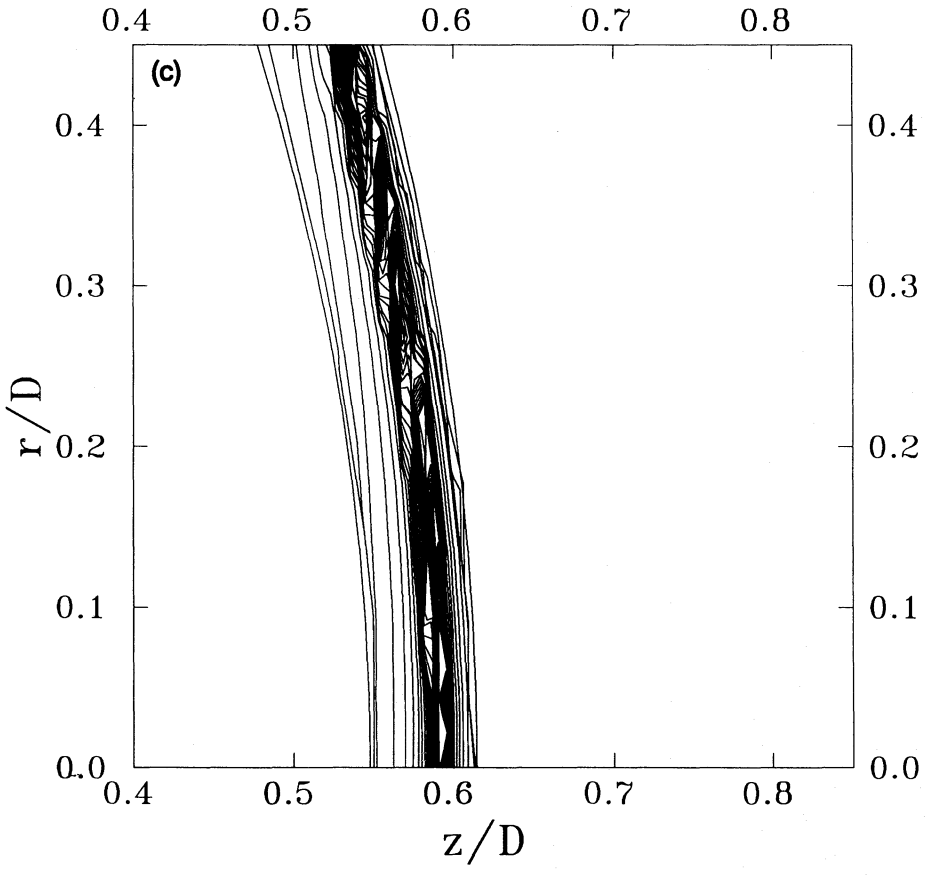

Figure 3 – *continued*

and Q_c in (9) influences the quantitative characteristics of the gas flow. Fig. 3 presents the isochores in the interaction region for $\Lambda = 6.25$ and $\chi = 0.78$, and the following sets of values for Γ_{ff} and Γ_c: $\Gamma_{ff} = \Gamma_c = 0$ (Fig. 3a); $\Gamma_{ff} = 0$, $\Gamma_c = 0.125$ (Fig. 3b); $\Gamma_{ff} = 0.125$, $\Gamma_c = 0$ (Fig. 3c). We can see in Fig. 3 that the influence of Comptonization is less than that of free–free emission. In fact, when $\Gamma_c = 0.125$, the thickness of the interaction region and the distribution of gas dynamical parameters differ slightly from those of the corresponding solution when $\Gamma_c = 0$. At the same time, an increase of Γ_{ff} from 0 to 0.125 causes a factor of 3 decrease in the shock region thickness near the axis of symmetry. This occurs because the energy losses by radiation gradually increase with the increase of the density and pressure, but the Comptonization directly depends only on the pressure distribution (the R_1 and R_2 values are changed slightly in the vicinity of the axis of centres). Furthermore, as can be seen in Fig. 3(a), the density increases across the shock regions I and II, so that the radiative cooling is most effective close to the contact discontinuity, and gives rise to high density gradients.

We have carried out two series of computations in order to check the accuracy of our model and to estimate the influence of the critical point (coincident with the stagnation point) on the solution in its vicinity.

In the first series, the number of grid points across each of the shock regions (I and II) was enlarged from 10 to 80. We can see in Fig. 4 that the increase of the number of grid points causes an infinite growth of density at the stagnation point ($\xi_2 = 0$) and does not actually influence the numerical solution when $\xi_2 > 0$ ($\xi_2 = [z - S(0)]/[G(0) - S(0)]$ is the relative position of the points on the axis of symmetry in region II). For $\xi_2 = 0$ the values of the pressure and the normal velocity component do not depend on the grid step, i.e. the use of boundary conditions (5) is correct. The positions and shapes of all the discontinuity surfaces do not depend on this step either.

In the second series, the magnitude of the numerical viscosity in the vicinity of the stagnation point was estimated with the help of the coefficient of artificial viscosity σ. When $\Gamma_{ff} \neq 0$ or $\Gamma_c \neq 0$, the numerical viscosity was found to be approximately equal to σ_* if the density values at the critical point in the cases of $\sigma = 0$ and $\sigma = \sigma_*$ differed from each other by more than 10 per cent. The value of the numerical viscosity estimated in this way decreases with the increase of the mesh number across the shock region. When $\Gamma_{ff} = 0.01$, and for 10 grid points in the z-direction of region II, therefore, σ_* is approximately equal to unity. In the case of 80 points, $\sigma_* \approx 0.1$. Thus these two calculation series testify that the distributions obtained of the gas pressure and the normal velocity component are correct over the whole region of the model, and the same is true for the density and the tangential velocity component, except for the area of the contact discontinuity. We note that the values of the density and the tangential velocity component at the contact surface do not influence the gas flow in the nearby region. This is why, in all the calculations, including the results demonstrated in Fig. 3, the values of these quantities are determined by an extrapolation.

The dependence of the geometrical structure on parameters L and χ is as follows. An increase of L causes an increase of Comptonization in both regions I and II due to the radiation from the second star. Consequently, the corresponding thicknesses Δ_I and Δ_{II} (at the axis of symmetry) decrease also, and the relation $\Delta_I/\tilde{\Delta}_I = \Delta_{II}/\tilde{\Delta}_{II}$ is fulfilled, where the tilde refers to the solution with $L = 1$. In the cases $\Gamma_{ff} \neq 0$ or $\Gamma_c \neq 0$, the dependence of the numerical solution on χ cannot be derived by a simple scaling as it can for the case of $\Gamma_{ff} = \Gamma_c = 0$. When $\Gamma_{ff} \neq 0$ and $\Gamma_c = 0$, the velocity increases with an increase of χ and the density decreases in region IV and consequently in region II (see equations 7 and 8). The role of energy losses in region II therefore decreases and Δ_{II} increases. In addition, the parameters of the gas flow in region I are actually unchanged. With the growth of χ the influence of Comptonization in region II decreases, because a velocity increase in region IV reflects an effective decrease of Γ_c.

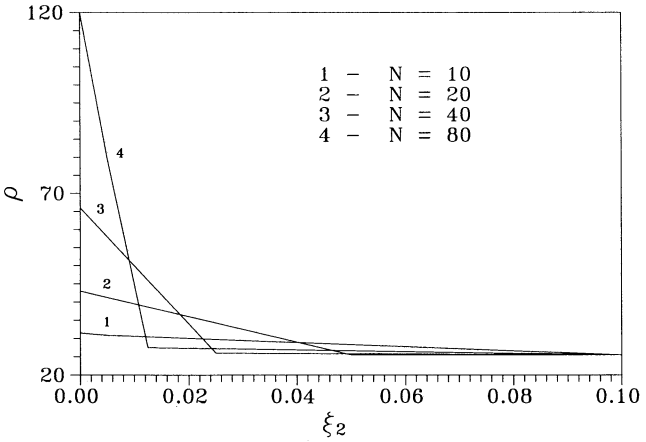

Figure 4. The dependence of the density at the stagnation point (region II) on the number of grid points across the slab.

As mentioned earlier, after deriving the solution in the subsonic and transonic regions ($r \leq r_0$) we continue it into the supersonic region ($r \geq r_0$) with initial conditions at $r = r_0$.

In the case $\Gamma_{ff} \neq 0$ and $\Gamma_c = 0$, the calculations of the gas flow parameters show that when $\Gamma_{ff} \ll 1$ the geometrical structure of the interaction region slightly differs from that at $\Gamma_{ff} = 0$ and $\Gamma_c = 0$, but this difference of gas dynamical parameters increases with distance from the axis of symmetry. Having this in mind, the density gradient at a distance $r = r_0$, which is insignificant at small values of Γ_{ff}, increases at greater distances, and at some $r = r_*(\Gamma_{ff})$ the numerical solution becomes unstable, but it is impossible to define whether this instability is physical or numerical. The critical value r_* decreases with the increase of Γ_{ff}. The heat-conductive gas model must therefore be considered in order to avoid the difficulties connected with the appearance of high gradients.

The influence of the Q_c term in the energy equation on the structure of the supersonic part of the interaction region is mainly defined by the initial conditions at $r = r_0$, because of the decrease of the role of Comptonization with the increase of distance from both stars. Furthermore, as already mentioned, the energy losses due to Comptonization have an almost even distribution across the shock region in comparison with those due to free–free emission. For this reason, the gas dynamical solution can be continued into the supersonic region at large distance, even for high values of Γ_c (Fig. 5). We can see in Fig. 5 that when $\Gamma_c \neq 0$ and $\Gamma_{ff} = 0$ all three

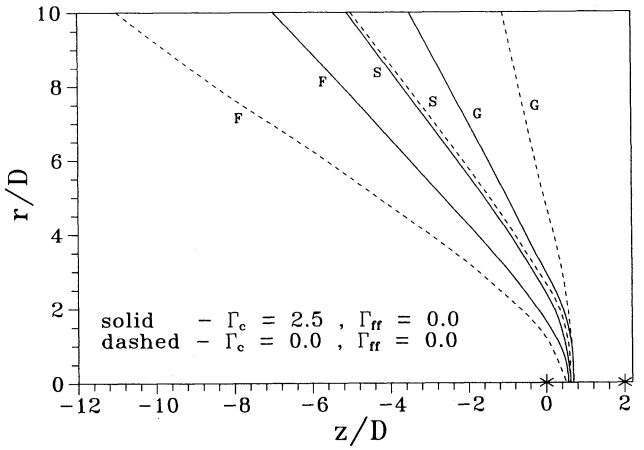

Figure 5. The dependence of the geometrical structure of the supersonic part of the interaction region on the Γ_c coefficient ($\Lambda_{ff}=6.25$, $\chi=1.0$, $K_1=K_2=0$).

discontinuities become linear at large distance from the axis of centres, as is in the case when $\Gamma_c=\Gamma_{ff}=0$, and the angle between the asymptotic directions of the F and G surfaces, i.e. the volume of the interaction region, decreases with the growth of Γ_c.

3.2 Effects of the stellar wind acceleration

The geometric structure and the distribution of the gas dynamical parameters in the interaction region strongly depend on the values of W and β in the case $K_1\neq 0$ or $K_2\neq 0$ (see Section 2). Let us consider two colliding stellar winds. The wind of star 1 obeys equations (7) and that of star 2 obeys equations (8). In the case that $K_2=0$ and $\chi=1$ it can be seen from (8) that

$$U=1, \qquad \rho=\dot{M}/R_2^2, \qquad p=0 \tag{10}$$

[we note that when $\Gamma_{ff}=\Gamma_c=0$ the dependence on χ is reduced to the same scaling as in the previous investigation (Lebedev & Myasnikov 1988)]. From equations (8) we can derive the Mach number in front of the F shock, M_F:

$$M_F^2=\left[1+\left(\frac{1}{W}-1\right)\left(1-\frac{K_1}{F_0}\right)^{\beta}\right]^{1+\alpha}\left(\frac{F_0}{K_1}\right)^{2(\alpha-1)}, \tag{11}$$

and increases with the decrease of W. In the case $W\ll 1$, therefore, which is interesting for massive-star winds, we obtain $M_F\gg 1$ if the F surface is not situated very close to the critical sphere H_1 where the flow velocity is equal to the sound speed. Then, using the Rayleigh formula (Myasnikov & Zhekov 1991) and the equations (8) and (10), we obtain, on the one hand, the relation between parameters F_0 and G_0 and, on the other hand, the dimensionless parameters of the gas dynamical problem:

$$(2-G_0)^2\left[W+(1-W)\left(1-\frac{K_1}{F_0}\right)^{\beta}\right]=\Lambda F_0^2, \tag{12}$$

where F_0 and G_0 are the distances from star 1 to the crossing points between the axis of symmetry and shocks F and G, respectively. If $M_F\geq 10$, all the numerical solutions satisfy this relation with an accuracy of about 1 per cent.

Substituting $S_0\approx F_0\approx G_0$ in (12), we obtain a non-linear equation in S_0:

$$W(2-S_0)^2+(1-W)\left(1-\frac{K_1}{S_0}\right)^{\beta}(2-S_0)=\Lambda S_0^2. \tag{13}$$

The numerical solution of this equation shows that the increase of β and K_1 and the decrease of W cause a shift of the contact discontinuity position for star 1 and, therefore, a shift of the whole shock region. These results are in good agreement with numerical $2D$ calculations.

The parameters β and W significantly influence the gas dynamical solution in the interaction region when $K_1\neq 0$. Fig. 6 presents the isochores in the shock region in the case of $K_1=0.2$, $\beta=1.35$ and $W=0.03$. In comparison with Fig. 3(a), it is seen that the density distribution in region I is significantly changed. This is the result of the different velocities (and, therefore, the densities) of the wind of star 1 in front of the F shock near the axis of symmetry and at great distance from it: $U=0.22$ and $U\rightarrow 1$, respectively. The effects of stellar wind acceleration therefore substantially influence the radiative characteristics of the interaction region (see Section 4.5).

4 X-RAY EMISSION FROM THE INTERACTION REGION

4.1 'Standard' source

In order to investigate the expected characteristics of the X-ray emission from binary systems that include massive stars losing mass in the form of a stellar wind, we shall consider the so-called 'standard' source. The 'standard' source class consists of WR and O stars and its main

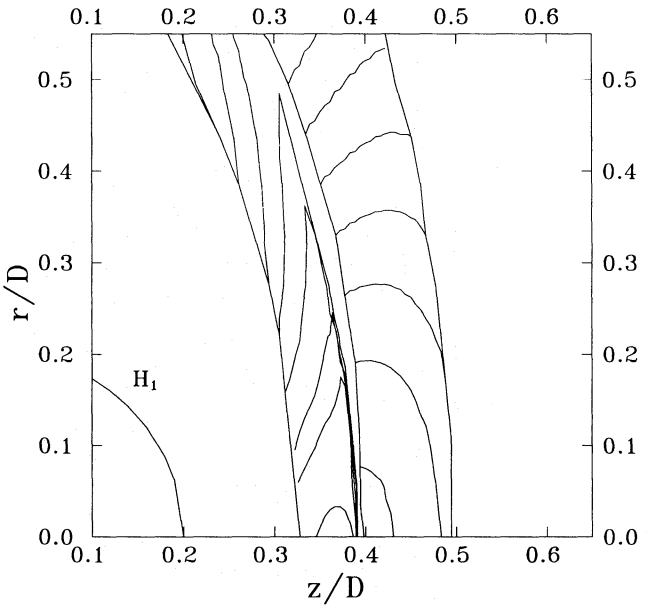

Figure 6. Isochores in the interaction region in the case with $\Lambda=6.25$, $\chi=0.78$, $\Gamma_{ff}=\Gamma_c=0$, $K_1=0.2$, $K_2=0$, $W=0.03$ and $\beta=1.35$. H_1 denotes the critical sphere, where $v_w=a_s$; a_s is the sound speed. The maximum values are near the axis of symmetry, z.

parameters have the following values:

$\dot{M}_1 = 1.6 \times 10^{-6}\,M_\odot\,yr^{-1}$, $\dot{M}_2 = 1.3 \times 10^{-5}\,M_\odot\,yr^{-1}$,

$v_{1\infty} = 2600\,km\,s^{-1}$, $v_{2\infty} = 2000\,km\,s^{-1}$,

$2D = 8 \times 10^{12}\,cm$,

where $\dot{M}_1$ and $\dot{M}_2$ are the mass-loss rates of the two stars, $v_{1\infty}$ and $v_{2\infty}$ are the terminal velocities of the winds (subscripts 1 and 2 refer to the O and WR stars, respectively) and $2D$ is the separation between the system components. In addition, we take into account the facts that the O-star wind (and, therefore, the gas in region I) has solar chemical composition and the WR-star wind (and therefore the gas in region II) consists of helium and heavier elements (see Section 4.2).

The dimensionless parameters determining the gas dynamical solution have the following values: $\Lambda = 6.25$, $\chi = 0.78$, $K_1 = 0.2$ and $K_2 = 0.07$. In region I $\Gamma_{ff} = 0.0035$, while in region II $\Gamma_{ff} = 0.004$ (for a WN star) or 0.002 (for a WC star). Γ_c values are between 0 and 5.

4.2 Chemical composition

WR stars are mainly divided into two types: WN (having nitrogen overabundance) and WC (having carbon overabundance). Enough information has been accumulated over the last few years to enable us to isolate a new type: WO (having oxygen overabundance) but, because of its rarity, we will not discuss this type further. One of the most important characteristics defining the main WR types is the chemical composition, and this can vary even within types (the differences are a factor of 2–3). To investigate the influence of the chemical composition on the X-ray emission of the 'standard' source, we use two average compositions, called the 'WN abundances' and the 'WC abundances'. To investigate their effect we use the recent reviews of Nugis (1990) and Willis (1990).

We assume that the atmospheres of both types are hydrogen-deficient, i.e. $N(H)/N(He) = 0$. Averaging the results given by Nugis (1991; every mean value weighted by the number of stars investigated) we find that the chemical composition (by number) of WN stars is $N(C)/N(He) < 2.5 \times 10^{-3}$, $N(N)/N(He) = 6.5 \times 10^{-3}$, while that of WC stars is $N(C)/N(He) = 0.244$, $N(O)/N(He) = 0.035$. On the other hand, using data from Willis (1991) the mean values for the WC type are $N(C)/N(He) = 0.353$, $N(C)/N(N) > 70$, $N(O)/N(He) < 7.9 \times 10^{-2}$. Averaging these results, we obtain the following composition (by number) for the WN type: $N(C)/N(He) = 1.44 \times 10^{-4}$ (we adopt the data from Willis, because Nugis gives only an upper limit), $N(N)/N(He) = 4.28 \times 10^{-3}$ and $N(O)/N(He) = 1.44 \times 10^{-4}$ [we assume $N(C)/N(O) \approx 1$ according to theoretical models, e.g. Maeder & Meynet 1987]. For the WC type we obtain $N(C)/N(He) = 0.299$, $N(N)/N(He) = 2.99 \times 10^{-3}$ [the value $N(C)/N(N) \approx 100$ is assumed, see above] and $N(O)/N(He) = 0.035$ (we adopt the Nugis data because Willis gives only an upper limit). Heavy-element abundances relative to helium are assumed to be solar (Allen 1973).

4.3 Ionization structure and X-ray emission

We calculate the ionization structure of the interaction region by taking into account collisional ionization by electrons and recombination (radiative and di-electronic), and by using an approximation of ionization equilibrium. The approximation is valid, because its characteristic time-scale is much less than the characteristic time-scale of the gas dynamical problem: $\tau = D/v_\infty \approx 10^4$ s at the typical temperature and nucleon density ($T \approx 10^{7-8}$ K, $n \approx 10^{8-11}$ cm^{-3}) in the shock region.

The X-ray spectrum and the luminosity of the interaction region are calculated using an approximation of optically thin plasma, and the gas emissivity integrated over the whole volume of regions I and II where the gas temperature is higher than 10^6 K. To determine the X-ray gas emissivity (erg cm^{-3}) we use the model of Raymond & Smith (1977), including free–free, two-photon and recombination continua, and emission lines of the following elements: H, He, C, N, O, Ne, Mg, Si, S, Ar, Ca, Fe and Ni. The different chemical compositions in regions I and II are also taken into account.

4.4 X-ray absorption in O-star and WR-star winds

Massive O-star and WR-star winds are efficient absorbers of the soft X-ray emission. In our model we take into account the X-ray absorption in the direction parallel to the z-axis. This is the maximum absorption, and it enables us to study its influence on the X-ray spectrum and the luminosity of the interaction region. Moreover, the majority of the known WR + O binary systems have inclination angles close to 90° (e.g. Aslanov et al. 1989). We assume that both the winds are relatively cool and that the chemical elements (except hydrogen and helium) are in different ionization stages, having filled up K-shells, so we consider only the K-shell absorption in our calculations. Optical and UV spectra of O and WR stars show that we have good reason to suppose this, and our assumption is also supported by radiation-driven wind models (Hellier 1987, 1989; Drew 1989).

We use the following form for the photoionization cross-section of H, He and He^+:

$$\sigma_\nu = a_\nu \left[\beta \left(\frac{E}{I} \right)^{-s} + (-\beta) \left(\frac{E}{I} \right)^{-s-1} \right],$$

where I is the ionization potential and E is the energy of an X-ray photon. The values of a_ν, β and s are given by Osterbrock (1974). To determine the cross-sections of the heavier elements, we follow Vanbeveren, van Rensbergen & de Loore (1982). The calculated cross-sections are multiplied by the relative abundances of the various elements and their sum represents the total photoionization cross-section at some energy. The different chemical compositions of O- and WR-star winds are taken into account. Fig. 7 shows the dependence of the total X-ray absorption cross-section on photon energy for different compositions of the wind gas. In these calculations, hydrogen is assumed to be fully ionized and helium is assumed to be mainly in the He^+ stage.

As mentioned above, to obtain the real X-ray spectrum and the luminosity of the interaction region, the 'net' spectrum of a gas slab, situated at a distance r from the axis of symmetry, is absorbed by the gas situated at the same distance in the O- and WR-star winds, respectively. For this purpose, the number density distribution is integrated in the corresponding direction, taking into account the ionization

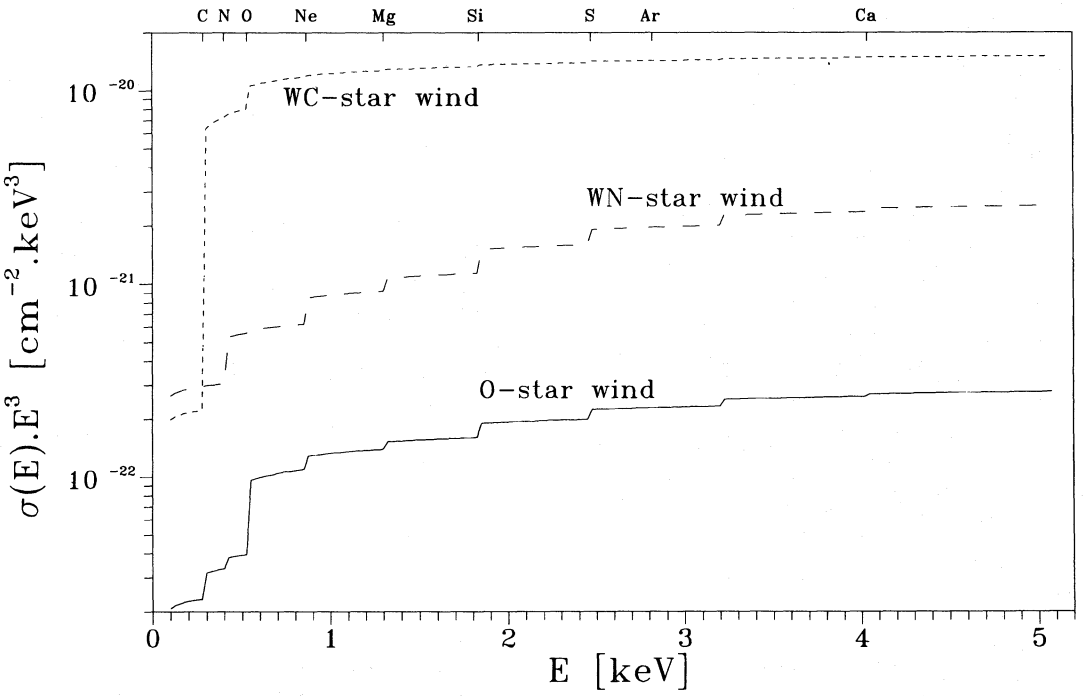

Figure 7. The total absorption cross-section for different chemical compositions: solar, WN and WC. The *K*-shell ionization edges of some elements are indicated.

structure (H, He, He^+) of both winds (Hillier 1987, 1989; Drew 1989). The column density thus calculated is used to determine the optical depth. The attenuated spectrum, $Sp(E)=Sp_0(E)\exp(-\tau_E)$, is sumined over all the slabs and the total X-ray spectrum and luminosity of the interaction region obtained.

In order to demonstrate the effects of X-ray absorption due to the interstellar medium, we use the model of Ride & Walker (1977), and the corresponding column density of hydrogen is estimated from the expression $N(\mathrm{H})=6\times10^{21}E(B-V)$ (Spitzer 1981).

4.5 Results

The X-ray luminosity and the spectrum (0.1–5 keV) of the interaction region have been calculated for two variants of the 'standard' source, namely two different chemical compositions of the WR component: 'WN abundance' and 'WC abundance'. The common assumption in all these calculations is that both winds have terminal velocities v_∞ in front of the shocks forming the interaction region. In all the remaining figures in this paper, the symbols 'WR – WR', 'WR – O', 'O – WR' and 'O – O' have the following meaning. The first part of each symbol denotes the emitting part (I or II) of the interaction region, i.e. WR denotes the shocked WR-star wind, and O denotes the shocked O-star wind. The second part of each symbol denotes the corresponding absorber: the WR-star wind or O-star wind, respectively.

Figs 8(a) and 9(a) present the dependence of the X-ray luminosity on the dimension of the interaction region in the *r*-direction (see Fig. 1). It can be seen that in both cases the whole of the luminosity is due entirely to the emission of the shocked gas of the WR stellar wind. As might be expected, the solution of the gas dynamical problem shows that the temperature and the particle density in region II are higher than those in region I. Another important result is that most of the X-ray luminosity originates in a region 2–3 times larger, in the *r*-direction, than the distance between the stars ($r/D=4$–6). The nearest section of the outlying part of the interaction region consists of a gas with a temperature ($T\approx1$–6×10^6 K) high enough to emit soft X-rays but, due to the relatively low number density, their contribution to the total luminosity is negligible. An exception occurs for the case in which the gas in region II has WC abundances and its X-ray emission is absorbed by the O-star wind. This occurs for the following reasons. First, in this case the gas temperature in region II is higher than that corresponding to WN abundances. Secondly, carbon is overabundant and its emission makes a considerable contribution in the spectral region $E>0.3$ keV; moreover, most of the total X-ray emission is found to be in the 0.3–1 keV energy range (Fig. 9b). Thirdly, the X-ray absorption due to the gas of the O-star wind, situated at distances from the axis of symmetry greater than $4D$, is insignificant ($\tau_{E<1\,\mathrm{keV}}\leq0.5$). Furthermore, we note that, when the WR-star wind gas has WN abundances, free–free and recombination continua supply about 23 per cent (19 and 4 per cent, respectively) of the total X-ray luminosity of the interaction region when X-ray absorption is due to the O-star wind, and about 56 per cent (39 + 17 per cent) in the case of WR-star wind absorption. For WC abundances, these contributions are 42 per cent (28 + 14 per cent) and 95 per cent (54 + 41 per cent), respectively. These listed values are naturally explained by the different chemical composition of the WR-star wind and by the fact that a considerable contribution to the total X-ray luminosity of the shock region is made by the line emission of

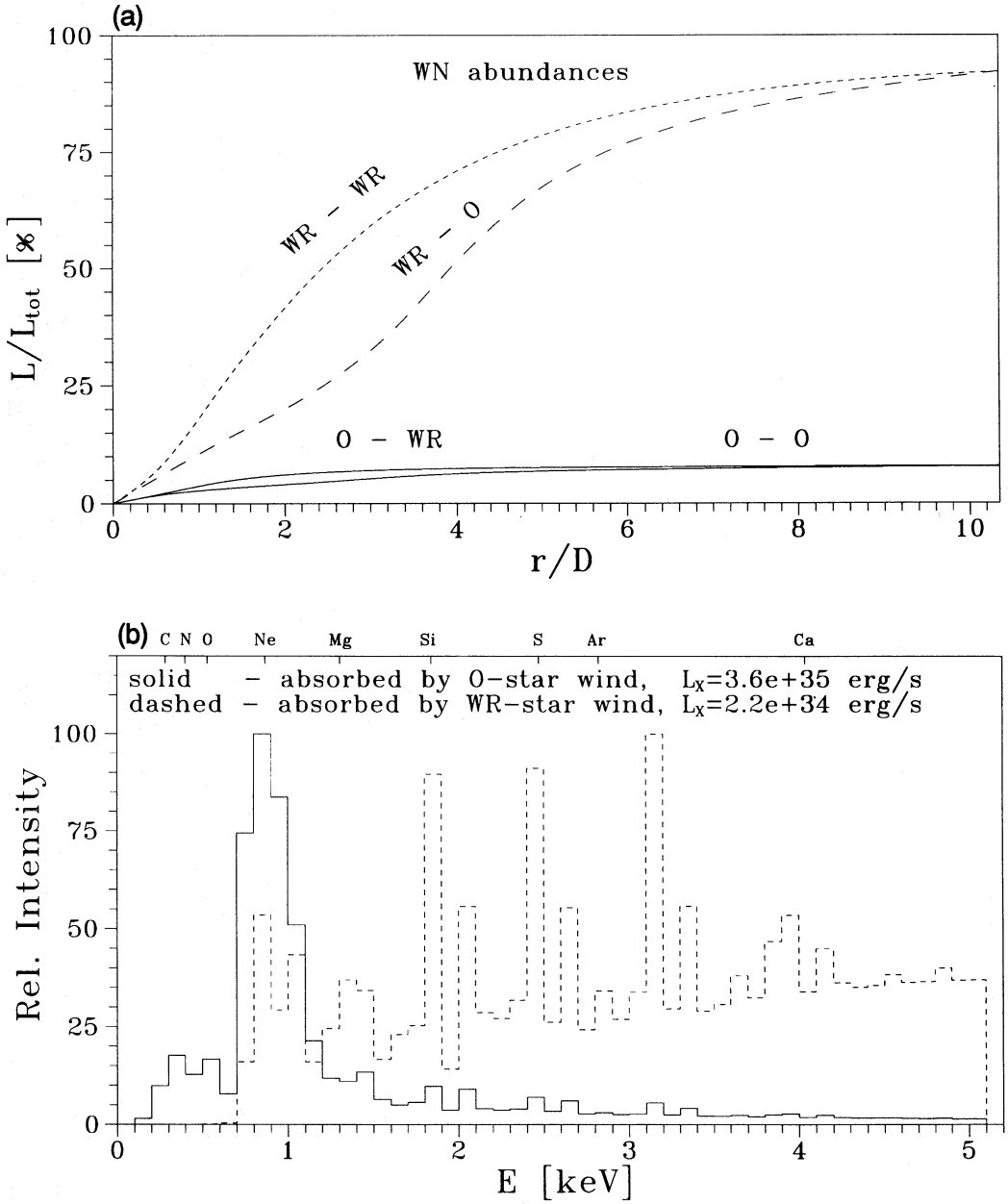

Figure 8. The X-ray emission characteristics of the interaction region in the case when the WR-star wind has WN abundances. (a) The dependence of the X-ray luminosity on the radius of the emitting region. The x-axis is in relative radial units, where $2D$ is the distance between the stars; the y-axis is in units of per cent. The labels 'WR − WR', 'WR − O', 'O − WR' and 'O − O' are explained in Section 4.5. (b) The X-ray spectrum attenuated by O-star wind absorption (solid line) and by WR-star wind absorption (dashed line); the X-ray luminosity in the 0.1–5 keV range is also given. The K-shell ionization edges of some elements are indicated.

energy about 1 keV (where the WR-star wind is a more efficient absorber; see Fig. 7). On the other hand, these results state that any approximate treatment of the problem of the X-ray emission from WR + O binary systems, which considers only a small region near the axis of symmetry and takes into account only free–free emission, significantly underestimates the X-ray luminosity of WR + O emitters.

The X-ray spectra for different chemical compositions of the WR component are shown in Figs 8(b) and 9(b). The attenuation due to the O- and WR-star winds is taken into account. In both cases the following characteristic feature exists: when the O component of the binary system is situated between the interaction region and the observer ('O star in front'), the maximum of the X-ray emission is at an energy of about 1 keV. As mentioned above, this maximum is mainly due to the powerful line emission of highly ionized species of different elements, e.g. Fe XVI–XXIV, Ni XIII–XIX, Mg XI, O VIII, Ne IX–X, etc. (see Raymond & Smith 1977). In addition, the spectral shape is significantly changed when the WR component is between the shock region and the observer ('WR star in front'): namely, the spectrum becomes harder and most of the emission is in the energy regions

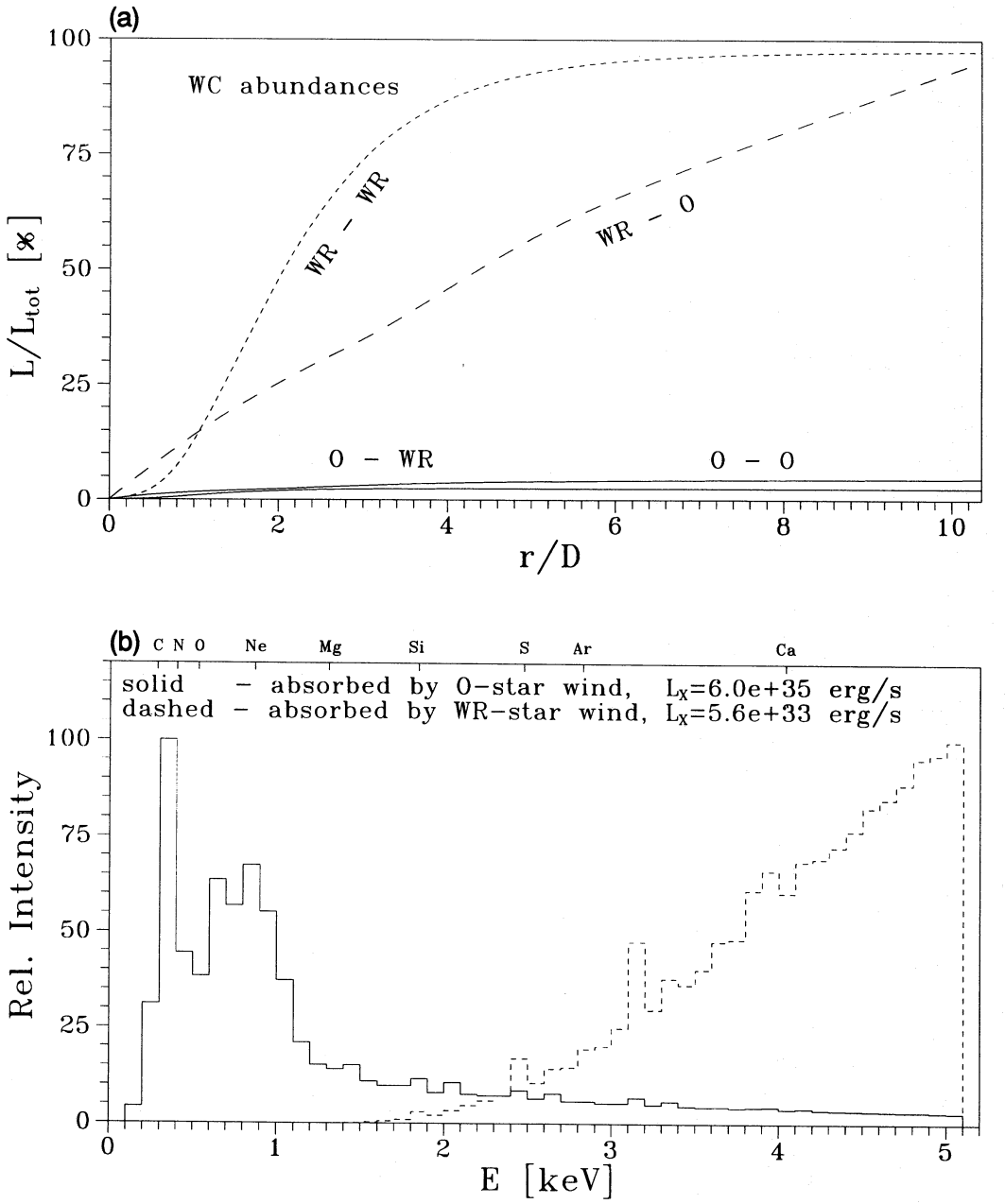

Figure 9. The X-ray emission characteristics of the interaction region in the case when the WR-star wind has WC abundances. (a) The dependence of the X-ray luminosity on the radius of the emitting region. The x-axis is in relative radial units, where $2D$ is the distance between the stars; the y-axis is in units of per cent. The labels 'WR − WR', 'WR − O', 'O − WR' and 'O-O' are explained in Section 4.5. (b) The X-ray spectrum attenuated by O-star wind absorption (solid line) and by WR-star wind absorption (dashed line); the X-ray luminosity in the 0.1–5 keV range is also given. The K-shell ionization edges of some elements are indicated.

$E > 1$ keV and > 2 keV for the cases of WN abundances and WC abundances, respectively. The X-ray luminosity (0.1–5 keV) in the case of 'O star in front' is about 15 times greater than in the case of 'WR star in front' when the WR stellar wind has WN abundances. This difference is about a factor of 100 when the WR stellar wind has WC abundances. All the changes occur because the elements He, C, N and O are overabundant in the WR-star wind, which is more massive than the O-star wind, i.e. the X-ray emission in the soft region ($E < 1$ keV) is entirely absorbed even at relatively large distances ($r/D \approx 8$–10) from the axis of the centres [$\tau_{E<1\,\mathrm{keV}} > 2$ for 'WN abundances' and $\tau_{E<1\,\mathrm{keV}} > 50$ for 'WC abundances'].

We have made an attempt to fit the theoretical spectra of the interaction region with isothermal models, often used in the analysis of X-ray observations. In order to simulate the observational situation more closely, i.e. to have about 10–15 points in the investigated spectral region, we have convolved the theoretical spectrum with *EXOSAT*-like filters having a Gaussian transmission curve with a full width at half-maximum of $\Delta E\,(\mathrm{keV}) = 0.5 E^{1/2}\,(\mathrm{keV})$ (*EXOSAT Observers Guide, 1985*). These results, in the case of WN abundances,

are shown in Fig. 10, in which all of the isothermal spectra are absorbed in both winds. We can see that none of the model spectra in Fig. 10 fits that of the interaction region in a satisfactory way. The best agreement is in the 1–1.5 keV energy range and exists only when the spectrum of an isothermal plasma, with a temperature of 10^7 K, is absorbed by an O-star wind gas. The isothermal approximations are not appropriate, therefore, when studying the X-ray emission from WR + O binary systems.

As demonstrated in Section 3.1, for WR + O binary systems the real values of Γ_{ff} have a negligible effect on the distribution of the physical parameters in the interaction region except in a thin region close to the contact discontinuity. On the other hand, larger values of Γ_{ff} require the introduction of thermal conductivity into the gas dynamical problem because of the occurrence of high thermal and density gradients. This is why all our calculations at $\Gamma_{ff} \neq 0$ may be used as estimates of the effects of energy losses by free–free emission; we do not consider their influence on the X-ray emission of the interaction region in this paper. In conclusion, we note that, for known WR + O binary systems (excluding very close ones like V444 Cyg, CQ Cep, CX Cep, etc.), Γ_{ff} takes very small values ($\Gamma_{ff} \leq 0.012$) and the X-ray luminosity is decreased by up to 10 per cent if energy losses by free–free emission are taken into account.

Energy losses by Comptonization ($\Gamma_c \neq 0$) have more

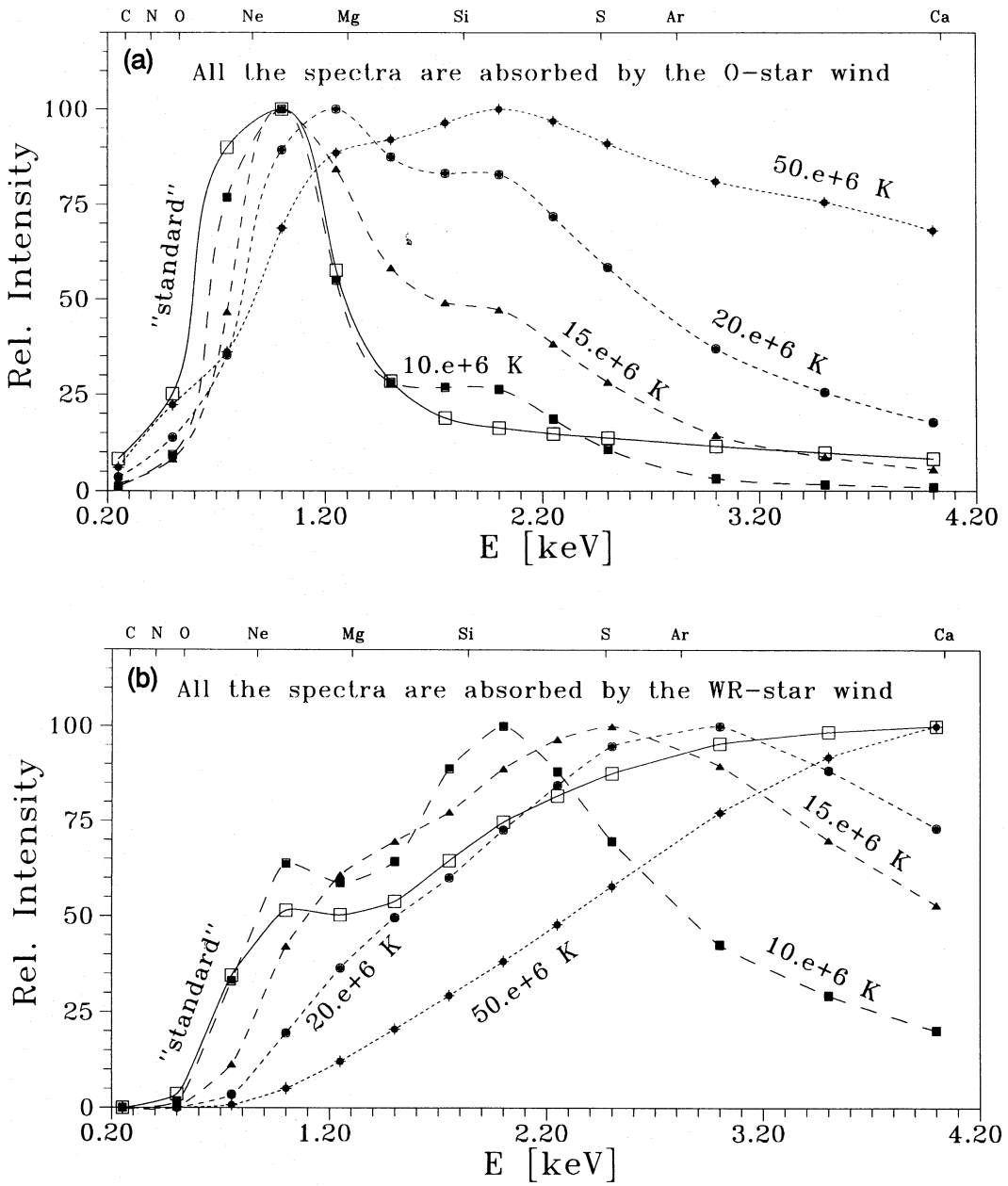

Figure 10. An approximation of the X-ray spectrum of the 'standard' source by isothermal sources (the temperature of the gas is indicated above each curve). All the spectra suffer the same attenuation. (a) Absorption is due to the O-star wind gas; (b) absorption is due to the WR-star wind gas. The *K*-shell ionization edges of some elements are indicated.

effect on the X-ray luminosity of the interaction region. Fig. 11 shows the dependence of the X-ray luminosity of the 'standard' source on Γ_c when the WR component of the binary system has WN abundances. This dependence may be explained as follows. An increase of Γ_c causes a decrease of the volume (V) of the interaction region and, as a result, the nucleon density grows ($n \propto V^{-1}$). The gas temperature also decreases, but it remains high enough for the shock region to be an X-ray source. This temperature decrease gives rise to an increase of the contribution of the low-energy photons ($E \approx 1$ keV) to the total luminosity, and causes a relative growth of the spectral lines in comparison to the continuum (free–free + recombination). Bearing these results in mind, and taking into account that (1) the luminosity is proportional to n^2V, and (2) the X-ray emission is efficiently absorbed at energies less than 1 keV, it is easy to see that with the increase of Γ_c the 'net' X-ray luminosity of the interaction region increases. In contrast, it decreases when the X-ray absorption due to O- and WR-star winds is considered (Fig. 11). For these reasons, the increase of Γ_c increases the dynamic range in the predicted values of the X-ray luminosity differences between the two cases of 'O star in front' and 'WR star in front'.

The next effect which must be considered in order to analyse the X-ray observations of WR + O binary systems is the X-ray absorption by the interstellar medium. The spectral shape in the case of the X-ray absorption by the WR-star wind (Figs 8b and 9b) shows that the spectrum will not be substantially changed by the X-ray absorption in the interstellar medium, because the absorption is most efficient at energies less than 1 keV. However, the interstellar absorption can significantly influence the spectral shape in other cases ('O star in front' etc.). As can be seen in Fig. 12, for the cases of WC abundances and 'O star in front', an increase of $E(B-V)$ (corresponding to an increase of the interstellar gas column density) causes a considerable change in the X-ray spectral shape of the 'standard' source: namely, the soft X-ray emission is reduced and, as a result, the spectrum becomes harder (the contribution of the $E \geq 1$ keV energy range to the total luminosity is increased). On the other hand, the X-ray luminosity of the interaction region decreases by only a factor of 3 when $E(B-V)$ increases from 0 to 1. The X-ray absorption by the interstellar medium will therefore decrease the dynamic range in the predicted values of the X-ray luminosity differences between the two cases of 'O star in front' and 'WR star in front'.

The picture is substantially different if at least one of the winds is not accelerated to its terminal velocity v_∞ in front of the shock. In order to demonstrate this effect, we consider the same 'standard' source (see Section 4.1) in the case of WN abundances, with the O-star wind obeying the law (6), where $W_1 = 0.03$, $\beta = 1.35$ and $v_{1\infty} = 2600$ km s^{-1}. We call this source the 'WN abundances + law'. The value of β is chosen to refer to an interaction region closer to the O star, and it corresponds to a decrease of the gas velocity in front of the $\vec{F}$ shock, i.e. to lower gas temperatures in region I (compressed O-star wind). The greater the value of β, the stronger are the effects of stellar wind acceleration. In fact, the values of β can have the following physical meaning in the case under discussion. Larger values of β mean that the stellar wind undergoes less acceleration, due to the O star, on the one hand, and to the WR-star radiation deceleration, on the other hand. As a result of O-star wind acceleration effects, the structure of the whole of region I is significantly changed, while the structure of the region II (compressed WR-star wind) is almost the same (see Figs 6 and 3a). For example, the maximum temperature is 100×10^6 K in the case of WN abundances, while it is 33×10^6 K in the case of WN abundances + law; the maximum nucleon densities are 1.6×10^{10} and 1.3×10^{11} cm^{-3}, respectively. All these changes cause an important growth of the contribution of region I to the total X-ray luminosity of the interaction region. They are valid mostly in the 'O star in front' case, whereas the status quo is unchanged in the 'WR star in front' case (compare Figs 13a and 8a). Comparing both cases, of WN abundances and WN abundances + law, one can see that the spectral shapes (0.1–5 keV) are not substantially different (Figs 13b, 8b). On the other hand, the X-ray

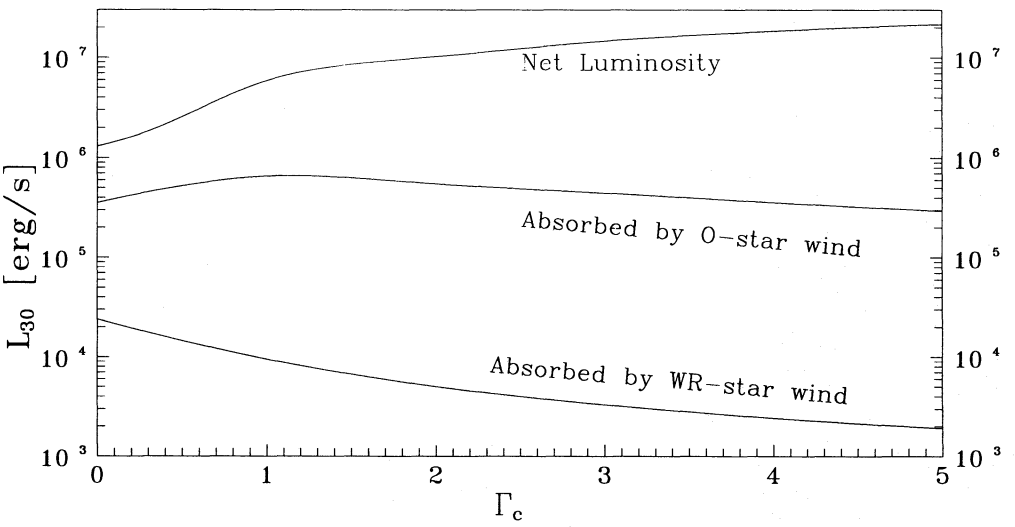

Figure 11. The dependence of the X-ray luminosity of the 'standard' source on the Γ_c coefficient. The K-shell ionization edges of some elements are indicated.

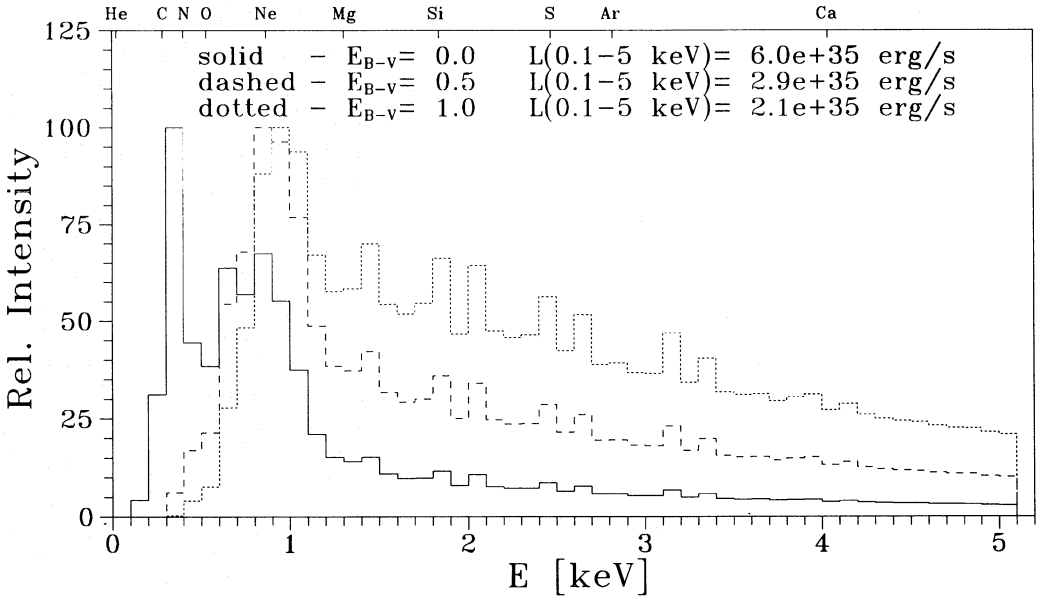

Figure 12. The X-ray spectrum of the 'standard' source for different values of interstellar absorption. The *K*-shell ionization edges of some elements are indicated.

luminosity (0.1–5 keV) in the case of 'O star in front' is about a factor of 40 higher than in the case of 'WR star in front', while this difference is about a factor of 15 when we have no acceleration effects (WN abundances). These results are not surprising, because the gas temperature decrease in region I causes a growth of the contribution to the total X-ray luminosity from the energy region at about 1 keV, and in this spectral range the WR-star wind is a strong X-ray absorber.

5 DISCUSSION

5.1 Common features

The results presented in Section 4.5 enable us to study the main characteristics of the X-ray emission from WR + O binary systems. The typical velocities of both winds in these systems suppose that the interaction region consists of high-temperature gas. Numerical simulations show that, if the WR + O binary system has 'standard' parameters (Section 4.1), the maximum temperature is about 10^8 K in region I, while in region II it is about 1.3×10^8 and 1.5×10^8 K in the cases of WN abundances and WC abundances, respectively (these temperatures will be lower if we take into account the effects of the stellar wind acceleration). Nevertheless, in the 'O star in front' case the existence of such high temperatures would not have been suspected by looking at the spectral shape in the 0.1–5 keV energy region (Figs 8b and 9b). They can be explained as follows. First, the hottest part of the interaction region occupies only a small volume near the axis of symmetry. Secondly, close to this axis the optical depth is greater than unity and most of the gas emission is absorbed by the O-star wind, so these parts of the shock region make only a small contribution to the total X-ray luminosity (Figs 8a and 9a). Thirdly, the spectral lines are very powerful in the energy region near 1 keV and they are the main contributors to the total luminosity. On the other hand, the spectral shape is also different in the 'WR star in front' case and, as mentioned above, this is due to the greater optical depth of the gas of the WR-star wind. The absence of an emission maximum above 2–3 keV in the observed spectra must not therefore be accepted as evidence for the absence of high temperatures (10^8 K) in the interaction region.

In addition, in view of the greater optical depth, the X-ray emission of a WC + O binary system will be harder than that of a WN + O binary system if the main parameters ($\dot{M}$, v_∞, D) have equal values.

If we assume that the stellar mass-loss rates are a factor of 10 less, the X-ray absorption in both winds will decrease, which will reduce the differences between the X-ray characteristics of the interaction region in the cases of 'O star in front' and 'WR star in front'. Fig. 14(a) demonstrates this in the WN abundances case: these differences are much less than the previous ones (see Fig. 8b). In addition, in the WC abundances case (Fig. 14b) the spectral shapes are still dissimilar for the different absorption conditions determined by the O-star and WR-star winds. Substantial emission has already appeared in the 2–4 keV energy region which was not seen earlier due to the WR-star wind absorption. The appearance of considerable emission in the 0.2–0.3 keV spectral region is a result of the relatively lower column density of the He^+ ion in the WC wind, compared to that in the WN wind (if both WR-star winds have equal values of the parameters $\dot{M}$, v_∞ and D), due to the overabundance of carbon (see Section 4.2). Moreover this emission is completely absorbed by the interstellar medium, even at small values of the colour excess, $E(B-V) \approx 0.1$–0.2. On the other hand, the appearance of the X-ray emission in the 0.2–0.3 keV energy range will be an additional tool, enabling us to investigate the mass loss and the chemical composition of a WR star, if we can observe a WC + O binary system which has $E(B-V)$ approximately equal to zero. For example, a small decrease of the relative abundance of

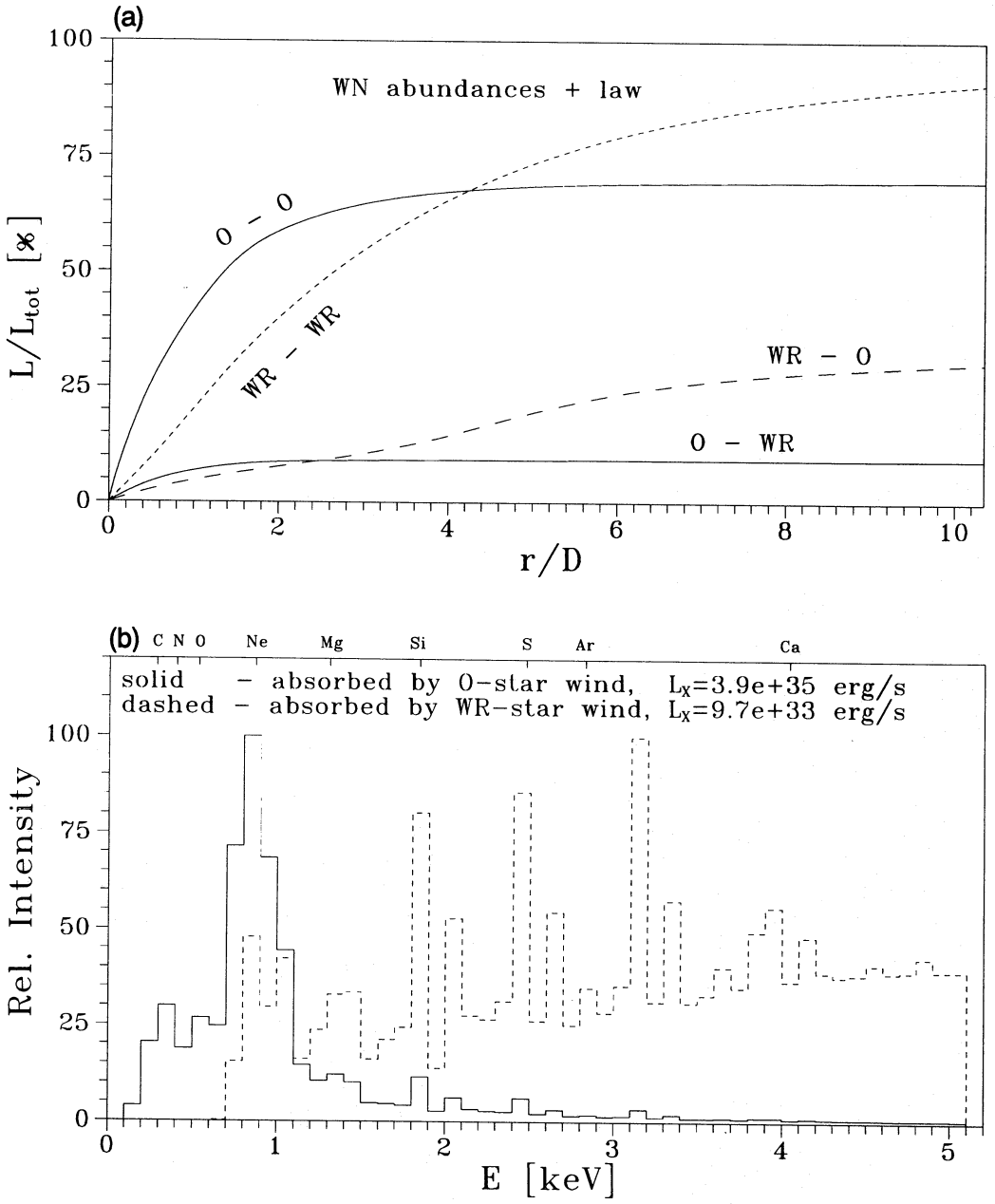

Figure 13. The X-ray emission characteristics of the interaction region for the case in which the WR-star wind gas has WN abundances and the effects of the stellar wind acceleration are taken into account. See captions to Figs 8 and 9 for explanation of symbols.

carbon will cause an increase of the He^+ ion column density, and this emission will be completely absorbed by the WR-star wind.

We can, therefore, obtain enough information about WR-star and O-star winds by studying the X-ray emission (spectrum + luminosity) from WR + O binary systems at different phases of their orbital motion. This information can be used for an independent estimate of the main physical characteristics of both stars, e.g. mass-loss rates and chemical compositions.

It is interesting to note that, with the increase of the contribution of the shocked O-star wind gas to the total X-ray luminosity (Fig. 13a), the ultraviolet (UV) luminosity (1000–2000 Å) of the interaction region also increases when the O-star wind acceleration effects are important. This UV increase is about a factor of 100 (from $\approx 3\times10^{33}$ to $\approx 4\times10^{35}$ erg s^{-1}) when the WR + O binary system has 'standard' parameters (see Section 4.1). In other words, the emission from the interaction region may be a significant fraction of the total UV luminosity of a WR + O system, and it can give the appearance of a UV variability (spectral and photometric) connected to the orbital motion (e.g. Shore & Brown 1988).

We therefore conclude that the closer a WR + O binary system is, the more significant are the effects of the stellar wind acceleration and the greater is the contribution of

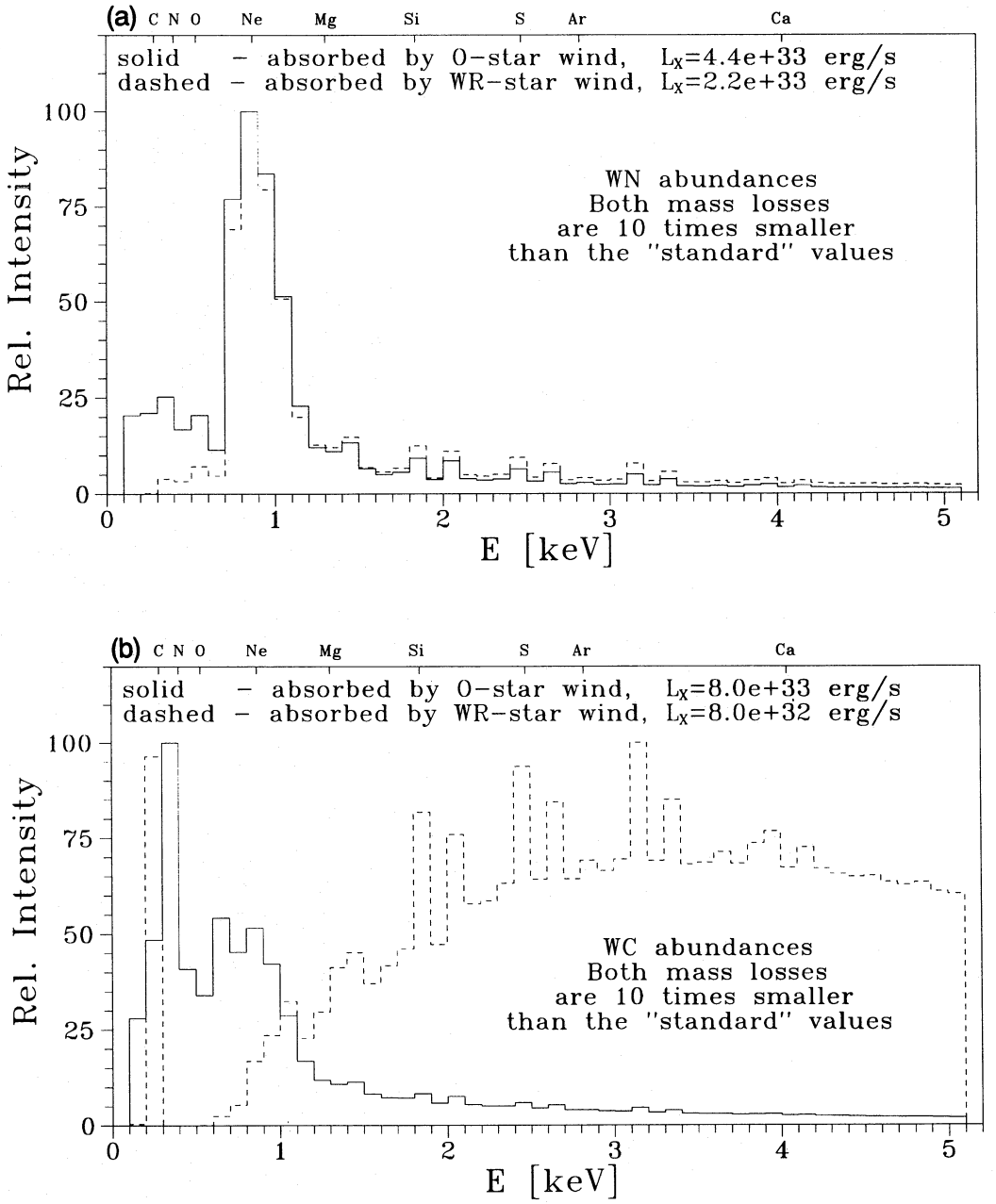

Figure 14. The X-ray spectrum of the interaction region for the case in which the mass-loss rate is a factor of 10 smaller than the 'standard' value. (a) WN abundances; (b) WC abundances. The X-ray luminosity in the 0.1–5 keV range is also given. The *K*-shell ionization edges of some elements are indicated.

region I to the total luminosity. In other words, it will be necessary to take this contribution into account in modelling the X-ray emission of these sources. Furthermore, close WR + O binary systems are probably more powerful UV sources than are single WR stars, and show spectral and photometric UV variability corresponding to the phase of their orbital motion.

On the other hand, the wider a WR + O binary system is, the greater is the possibility that both winds will reach their terminal velocities in front of the F and G shocks forming the interaction region. This is why the temperature of the shocked gas will be higher in these systems, and why they will be harder X-ray sources than will close WR + O binaries.

All the variants of the 'standard' source that we have considered show that one of the most important parameters determining the X-ray spectral shape and luminosity of a WR + O binary system is the X-ray absorption depth of the O-star and WR-star wind gases, respectively. Apart from the chemical composition, the absorption also depends on the geometry, i.e. on the inclination angle between the orbital plane and the line of sight. The smaller this angle is (it is equal to 90° when the line of sight coincides with the line of

centres), the smaller is the X-ray absorption in both winds. This means that the X-ray emission of these systems will be more powerful and softer in comparison with that of WR + O binaries, having an inclination angle close to 90° if the physical characteristics ($\dot{M}$, v_∞, D) of the systems are not different.

It is important to note that, in all cases of massive binary systems (WN + O, WC + O, WR + WR, etc.), most of the X-ray emission ($E > 0.1$ keV) from the interaction region is absorbed by the O-star and WR-star wind gas. The power of this absorbed radiation is $L_{x(\text{absorbed})} \geq 10^{36}$ erg s^{-1} for typical values of $\dot{M}$, v_∞ and D. Due to its relatively large value, the absorbed energy can influence the ionization structure of both winds. Taking into account the fact that the ionization energies of the heavier and most abundant elements like C, N and O are in the same energy region ($E > 0.1$ keV), we can deduce that the binary WR stars must have more intensive spectral lines of highly ionized species of different chemical elements in comparison with the single WR stars.

5.2 Scaling laws

There are some common laws (Luo et al. 1990) which make possible the estimation of the 'net' X-ray luminosity of the interaction region at different values of the main physical parameters derived from observations ($\dot{M}_2$, $v_{2\infty}$, D). For example, the total X-ray luminosity L_x is proportional to $n^2 T^{-0.6} V$, where n, T and V are the nucleon density, the gas temperature and the volume of the shock region, respectively. Moreover, from the continuity equation and the relation between the temperature and the wind velocity at the shock surface, it follows that $L_x \propto \dot{M}_2^2 v_{2\infty}^{-3} D^{-1}$. Our numerical simulations have confirmed this result. The power-law index of $v_{2\infty}$ is equal to -2.90 or -3.3, depending on the chemical composition. However, the real X-ray luminosity of the interaction region, i.e. that influenced by the X-ray absorption in O- and WR-star winds, does not obey this scaling law.

In order to investigate the L_x dependence on different dimensional quantities, we have kept the dimensionless parameters $\dot{M} = \dot{M}_2/\dot{M}_1$, $\chi = v_{2\infty}/v_{1\infty}$ and $\Lambda = \dot{M}\chi$ unchanged, because they determine the structure of the interaction region (see Section 3). Considering the case of an O-star wind absorption, our calculations show that the total X-ray luminosity of the shock region shows the following dependences. On the mass-loss rate: $L_x \propto \dot{M}_2^{-1.8}$ ($10^{-6} \leq \dot{M}_2 \leq 8 \times 10^{-5}$ $M_\odot$ yr^{-1}); on the wind velocity: $L_x \propto v_{2\infty}^{-2.6}$ and $v_{2\infty}^{-2.9}$ in the cases of WN abundances and WC abundances, respectively ($1500 \leq v_{2\infty} \leq 4000$ km s^{-1}); on the separation between stars: $L_x \propto D^{-0.8}$ ($10^{12} \leq D \leq 3 \times 10^{13}$ cm). On the other hand, from studying the case of WR-star wind absorption, these dependences might best be approximated by a logarithmic function or a second-order polynomial. These differences can be explained as follows. In all cases the X-ray luminosity L_x roughly consists of two parts, corresponding to the 'net' luminosity and the wind absorption, i.e.

$$L_x \propto \dot{M}_2^2 \exp(-\alpha \dot{M}_2), \qquad L_x \propto D^{-1} \exp(-\beta/D),$$

$$L_x \propto v_{2\infty}^{-2.9,\,-3.3} \exp(-\gamma/v_{2\infty}).$$

The common feature of these dependences is that a maximum of X-ray luminosity has to exist at any characteristic value of $\dot{M}_2$, $v_{2\infty}$ and D. These characteristic values depend on the dimensionless parameters $\dot{M}$, χ and Λ, as well as on the chemical composition. Our numerical calculations have confirmed the existence of maximum values of L_x. When small ranges of dimensional parameters are considered, therefore, we can obtain different parts of the above mentioned dependences and they can then be successfully approximated by various functions: exponential, logarithmic, polynomial, etc.

These results conclusively show that the 'scaling laws' connecting the total X-ray luminosity L_x with the main dimensional parameters $\dot{M}_2$, $v_{2\infty}$ and D have limited applications. In other words, for any WR + O binary system we have to determine its X-ray emission on the basis of the numerical solution of the gas dynamical problem, giving the structure of the interaction region at the particular values of the dimensionless parameters $\dot{M}$, χ, Λ, Γ_{ff} and Γ_c.

5.3 Perspectives

Future X-ray observations, having good spectral resolution and sensitivity, will enable us to study WR + O binary systems in detail. These observations are of particular interest when investigating the variation of the X-ray flux and the spectrum as functions of different phases of the orbital motion. We shall thus be able to use the X-ray emission of the interaction region like a probe, giving an independent check on information obtained from other observations (radio, IR, optical, UV) about mass-loss rates and chemical compositions of both stars.

On the other hand, solutions of the gas dynamical problem (Sections 2 and 3) can be used to model the X-ray emission of other binary systems consisting of massive stars with stellar winds, i.e. WR + WR, O + O, O + B.

It is very interesting to consider this problem in the context of a binary system in which one of the components is a young hot star with a high-velocity stellar wind ($v_\infty > 1000$ km s^{-1}), and its companion is a late-type star with a slow and massive wind ($v_\infty \sim 10$–20 km s^{-1}). In this case, both parts (I and II) of the interaction region will emit mainly in different spectral regions: the section consisting of a shocked high-velocity stellar wind will be a powerful X-ray source, while the other section will be an optical source. This binary system will therefore probably display X-ray and an optical variability, as well as strong spectral lines of highly ionized species of different chemical elements.

6 CONCLUSIONS

We have performed two-dimensional calculations of colliding stellar winds in a WR + O binary system. We summarize our results and conclusions below.

(1) We see from Section 4.5 that the energy losses by free–free emission underestimate the total energy losses due to thermal emission. Nevertheless, it is important that free–free emission losses be studied in order to investigate the influence of the thermal emission losses on the structure of the interaction region. Large values of Γ_{ff} lead to the appearance of high density (temperature) gradients. To include all the thermal emission losses, therefore, Γ_{ff} must be effectively increased. The *only* correct gas dynamical problem is then this one, taking into account the thermal conductivity. However, for typical WR + O binary systems

(excluding very close ones such as V444 Cyg, CQ Cep, CX Cep, etc.), $\Gamma_{ff} \approx 0.01$ and the role of Γ_{ff} in X-ray emission can be neglected. On the other hand, Γ_c is more important in this case and has to be taken into account in the modelling of the X-ray emission.

(2) The stellar wind acceleration effects can substantially change the gas dynamical parameters in the interaction region and, therefore, the X-ray emission. These effects are very important for close WR + O binary systems, in which the contribution of the shocked O-star wind gas to the total X-ray emission may be dominant.

(3) One of the most important parameters determining X-ray emission from the interaction region is the optical depth of both winds, which depends strongly on their chemical composition. X-ray observations of WR + O binary systems, investigating their spectra and flux variability and combined with X-ray emission modelling, will be a powerful tool in the study of the physical parameters of both stars. X-ray observations may be used in the determination of the mass-loss rates and the chemical compositions, independent of the results of radio, infrared, optical and UV observations.

(4) The presence of the interaction region and its X-ray emission can substantially influence the ionization structure of both winds. This is why the spectra of binary WR stars must show more intensive spectral lines of high-ionization species of different chemical elements in comparison with single WR stars.

(5) No scaling laws exist that give a relation between the total X-ray luminosity and the main dimensional parameters: mass-loss rates, stellar wind velocities and stellar separation. In other words, for every WR + O binary system we must determine the X-ray emission on the basis of the numerical solution of the corresponding gas dynamical problem.

In a future paper, we intend to calculate the expected X-ray emission of WR + O and O + O binaries that are most important from the observational point of view, i.e. those having good estimates for the main physical parameters (mass-loss rates, wind velocities, separation between stellar components).

ACKNOWLEDGMENTS

The authors wish to thank Professor V. B. Baranov for his interest in this work and for initiating the authors' collaboration, and Dr N. G. Bochkarev and Professor A. M. Cherepashchuk for useful discussions. SAZ thanks the leadership of the Special Astrophysical Observatory (Nizhnij Arkhyz) and Sternberg State Astronomical Institute for the financial support and the hospitality which enabled him to spend two months in Moscow where this work was initiated. AVM thanks the leadership of the Space Research Institute (Sofia) for its financial support during his stay in Sofia where this work was finished. We also wish to thank Dr R. McCray for reading the manuscript and making helpful comments. The authors thank an anonymous referee for valuable comments and criticism.

NOTE ADDED IN PRESS

Our attention has been drawn by the referee to the recently published paper by Stevens, Blondin & Pollock (1992). We should like to comment upon it. Very valuable investigations of the X-ray emission from WR + O binary systems, as well as the instability of the shocked gas region, are presented in Stevens et al. They study self-consistently the effects of all the thermal emission losses (continuum and emission lines) on the characteristics of the interaction region. The main difference between their paper and ours is that we use a shock-fitting method for two-dimensional calculations, while they carry out two-dimensional calculations with the help of a shock-capturing method. With our method, we are able simultaneously to take into account the different chemical compositions in both winds, which was not possible in their calculations, as noted in the paper. We include in our gas dynamical calculations the energy losses by free–free emission only, and this is an underestimate of the total thermal emission losses. On the other hand, it is enough merely to have an idea about the influence of the thermal energy losses on the structure of the shocked gas region, and our calculations show the appearance of high density (temperature) gradients near the contact discontinuity. The only correct way to include all the thermal emission losses is then to take into account the thermal conductivity. In contrast, all the results must be treated with caution, because these high gradients may influence the physical characteristics of the whole interaction region, especially if the number of grid points in the r-direction (Fig. 1) across the interaction region itself is not too large (as it probably is in the calculations of Stevens et al.). In our opinion, therefore there is no preference for either of the two main methods of calculation (shock fitting and shock capturing), and their results are complementary. In addition, all model calculations of colliding stellar winds show that it is a very interesting problem, description of which requires the application of complex physics.

REFERENCES

Allen C., 1973, Astrophysical Quantities. 3rd edn, The Athlone Press, London

Aslanov A. A., Kolosov D. E., Lipunova N. A., Hruzina T. S., Cherepashchuk A. M., 1989, in Cherepashchuk A. M., ed., Katalog tesnyh dvoinyh zvezd na pozdnih stadiyah evolutsii. Moscow State University Press, Moscow, p. 53

Babenko K. I., Rusanov V. V., 1965, in Trudy II Vsesouznogo s'ezda po theoreticheskoi i prikladnoi mechanike. No. 2, Nauka, Moscow, p. 247

Bajramov Z. I., Pilyugin N. N., Usov V. V., 1988, Astron. Tsirk., 1526, 1

Bajramov Z. I., Pilyugin N. N., Usov V. V., 1990, AZh, 67, 998

Beals C. S., 1929, MNRAS, 90, 202

Bogopelov V. V., Neiland V. Ya., 1966, Fluid Dyn., 1, No. 5, 15

Cherepashchuk A. M., 1967, Perem. Zvezdy, 16, 226

Cherepashchuk A. M., 1976, Pis'ma Astron. Zh., 2, 356 (English translation in Sov. Astron. Lett., 2, 138)

Cherepashchuk A. M., 1990, AZh, 67, 955

Chernij G. G., 1959, Techenie gaza s bol'shoy sverhzvukovoy skorost'yu. Fizmatgiz, Moscow

Conti P. S., 1988, in Conti P. S., Underhill A. B., eds, O Stars and WR Stars. NASA SP-497, p. 81

Coulard R., 1964, Am. Inst. Aeronaut. Astronaut. J., 2, 494

Drew J. E., 1989, ApJS, 71, 267

Dyakonov Yu. N., Uskov V. I., 1970, Nauchnye Trudy Instituta Mechaniki MGU, No. 5, Moscow State University Press, Moscow, p. 73

Girard T., Wilson L., 1987, A&A, 183, 247

Hillier D. J., 1987, ApJS, 63, 947
Hillier D. J., 1989, ApJ, 347, 392
Kallrath J., 1991, MNRAS, 248, 653
Lebedev M. G., Myasnikov A. V., 1988, in Paskonov V. M., Roslyakov G. S., eds, Numerical Methods in Aerodynamics. Moscow State University Press, Moscow, p. 3
Lebedev M. G., Myasnikov A. V., 1990, Izvestia Akademii Nauk SSSR – Mekhanika Zhidkosti i Gaza, No. 4, 159 (English translation in Fluid Dyn., 1990, 25, No. 4)
Lebedev M. G., Sandomirskaya I. D., 1981, Vichistlitel'nie metody i programirovanie, Vol. 34, Moscow University Press, Moscow, p. 70.
Levich E. V., Sunyaev R. A., 1971, AZh, 48, 461 (English translation in SvA – AJ, 15, 363)
Luo D., McCray R., Maclow M.-M., 1990, ApJ, 362, 267
Maeder A., Meynet G., 1987, A&A, 182, 243
Moffat A. F. J., Firmani C., McLean I. S., Segewiss W., 1982, in de Loore C. W. H., Willis A. J., eds, Proc. IAU Symp. 99, Wolf–Rayet Stars: Observations, Physics, Evolution. Reidel, Dordrecht, p. 577
Myasnikov A. V., Zhekov S. A., 1990, Astron. Tsirk., 1545, 1
Myasnikov A. V., Zhekov S. A., 1991, Ap&SS, 184, 287
Nugis T., 1991, in Michaud G., Tutukov A., eds, Proc. IAU Symp. 145, Evolution of Stars: The photospheric Abundance Connection. Reidel, Dordrecht, p. 209
Osterbrock D. E., 1974, Astrophysics of Gaseous Nebulae. W. H. Freeman and Company, San Francisco
Pollock A. M. T., 1987, ApJ, 320, 283
Prilutskii O., Usov V. V., 1976, AZh., 56, 6 (English translation in SvA – AJ, 20, 2)
Raymond J. C., Smith B. W., 1977, ApJS, 35, 419
Ride S. K., Walker A. B. C., 1977, A&A, 61, 339
Shima E., Matsuda T., Inaguchi T., 1986, MNRAS, 231, 687
Shore S. N., Brown D. N., 1988, ApJ, 334, 1021
Siscoe G. L., Heinemann M. A., 1974, Ap&SS, 31, 363
Spitzer L., 1962, Physics of Fully Ionized Gases. 2nd edn, Interscience, New York.
Spitzer L., 1978, Physical Processes in the Interstellar Medium. Wiley, New York
Stevens I. R., Blondin J. M., Pollock A. M. T., 1992, ApJ, 386, 265
Stulov V. P., Shapiro E. G., 1969, Fluid Dyn., 4, No. 2, 48
Stulov V. P., Shapiro E. G., 1970, Fluid Dyn., 5, No. 1, 140
Thomas P. D., 1965, Am. Inst. Aeronaut. Astronaut. J., 3, 1401
Vanbeveren D., van Rensbergen W., de Loore C., 1982, A&A, 115, 69
Vertushkin V. K., Zhigulev N., 1967, Fluid Dyn., 2, No. 2, 17
Willis A. J., 1991, in Michaud G., Tutukov A., eds, Proc. IAU Symp. 145, Evolution of Stars: The Photospheric Abundance Connection. Reidel, Dordrecht, p. 195
Zhekov S. A., Myasnikov A. V., 1989, Astron. Tsirk., 1537, 13